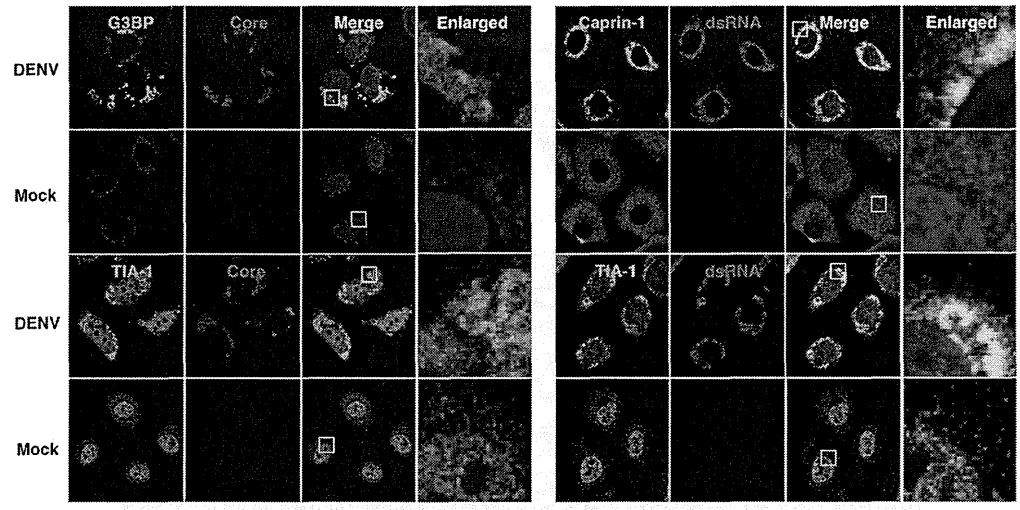

FIG 3 Subcellular localizations of the SG-associated proteins during DENV infection. Cellular localizations of G3BP, Caprin-1, and TIA-1 (green, AF488-conjugated secondary antibody) and viral components (core protein and dsRNA) (red, AF-594-conjugate secondary antibody) in Huh7 cells infected with DENV were determined by immunofluorescence analysis using the appropriate antibodies at 48 h postinfection. Cell nuclei were stained with DAPI (blue).

Preparation of recombinant proteins and GST pulldown assay. His-tagged JEV core protein (core-His) was purified as described in a previous report (25). Briefly, core-His was expressed in *Escherichia coli* (*E. coli*) Rosetta-gami 2(DE3) strain cells (Novagen-Merck) transformed with pET21b-Core-His (WT or 9798A). Bacteria grown to an optical density at 600 nm of 0.6 were induced with 0.5 mM isopropyl-β-D-thiogalactopyranoside (IPTG), incubated for 5 h at 37°C with shaking, collected by centrifugation at 6,000 × *g* for 10 min, lysed in 10 ml of bacteria lysis buffer (50 mM Tris-HCl, pH 7.4, 150 mM NaCl, 1 mM EDTA, 1% Triton X-100, and protease inhibitor cocktail [Complete; Roche]) by sonication on ice, and centrifuged at 10,000 × *g* for 15 min. The supernatant containing core-His was subjected to ammonium sulfate fractionation, followed by cation exchange chromatography with a HiTrap SP column (GE Healthcare). The eluted core-His recombinant protein was dialyzed with 50 mM Tris-HCl buffer containing 150 mM NaCl at 4°C overnight. GST-fused Caprin-1 (GST-Caprin-1) was expressed in *E. coli* BL21(DE3) cells transformed with pGEX-GST-Caprin-1. Bacteria grown to an optical density at 600 nm of 1.0 were induced with 0.1 mM IPTG, incubated for 5 h at 25°C with shaking, collected by centrifugation at 6,000 × *g* for 10 min, lysed in 10 ml of bacteria lysis buffer by sonication on ice, and centrifuged at 10,000 × *g* for 15 min. The supernatant was mixed with 200 μl of glutathione-Sepharose 4B beads (GE Healthcare) equilibrated with bacteria lysis buffer for 1 h at room temperature, and then the beads were washed five times with lysis buffer. Twenty micrograms of GST-Caprin-1 or GST was mixed with equal volumes of the purified core-His for 2 h at 4°C with gentle agitation. The beads were washed five times with bacteria lysis buffer and then suspended in SDS-PAGE sample buffer.

Mouse experiments. Experimental infections were approved by the Committee for Animal Experiment of RIMD, Osaka University (H19-2-0). Female ICR mice (3 weeks old) were purchased from CLEA Japan (Tokyo, Japan) and kept in specific pathogen-free environments. Groups of mice ($n = 10$) were intraperitoneally inoculated with 5×10^4 FFU (100 μl) of the viruses. The mice were observed for 3 weeks after inoculation to determine survival rates. To examine viral growth in the brain, 5×10^4 FFU of the viruses were intraperitoneally administered to the groups of mice ($n = 3$). At 7 days postinfection, mice were euthanized, and the cerebrums were collected. The infectious titers in the homogenates of the cerebrums were determined in Vero cells as described above.

RESULTS

JEV infection confers resistance to SG induction. To examine the formation of SGs in cells infected with JEV, Huh7 cells were infected with JEV at a multiplicity of infection (MOI) of 0.5, and the expression of JEV proteins and an accepted marker for SGs, G3BP, was determined by immunofluorescence analysis at 24 h postinfection. G3BP was mainly accumulated in the perinuclear region and partially colocalized with the JEV core protein, while only partial colocalization with the NS2B protein was also observed (Fig. 1A, left). In addition, a few small G3BP-positive foci were scattered in the cytoplasm. This accumulation of G3BP was observed in not only Huh7 cells but also other cell lines, i.e., 293T and HeLa cells, infected with JEV (Fig. 1B). However, the expression level of G3BP in cells infected with JEV was comparable to that in mock-infected cells (Fig. 1C). To further investigate SG induction by JEV infection, expression of TIA-1, another SG marker, was examined. Although accumulation of TIA-1 in the perinuclear region was not observed, a few TIA-1-positive foci were observed in the JEV-infected cells and were colocalized with G3BP and JEV NS2B, indicating that SG foci were induced in cells infected with JEV (Fig. 1D). The accumulation of G3BP and the aggregation of TIA-1, indicating SG formation, appeared at 24 h postinfection in accord with the expression of viral proteins (Fig. 1E). We further examined the dynamics of other SG-associated factors in cells infected with JEV. Each factor formed clear SGs in cells treated with sodium arsenite, a potent SG inducer eliciting oxidative stress (Fig. 2). As shown in Fig. 1F, three distinct patterns of the subcellular localization of SG components were observed. USP10 and Caprin-1 were accumulated in the perinuclear region and also formed a few small foci scattered throughout the cytoplasm, as seen for G3BP; TIA-1 and hnRNP Q formed cytoplasmic foci but were not accumulated in the perinuclear region; and subcellular localization of eIF3A and eIF4B was not changed. The cytoplasmic foci were confirmed as SGs by immunofluorescence analyses using specific antibodies to SG-associated factors (data not shown). Taken together, these results indicate that JEV infection induces accumulation of several RBPs and formation of a few SGs.

It has been shown previously that infection with WNV or DENV confers resistance to SG formation induced by sodium arsenite (15). To determine the effect of JEV infection on the SG

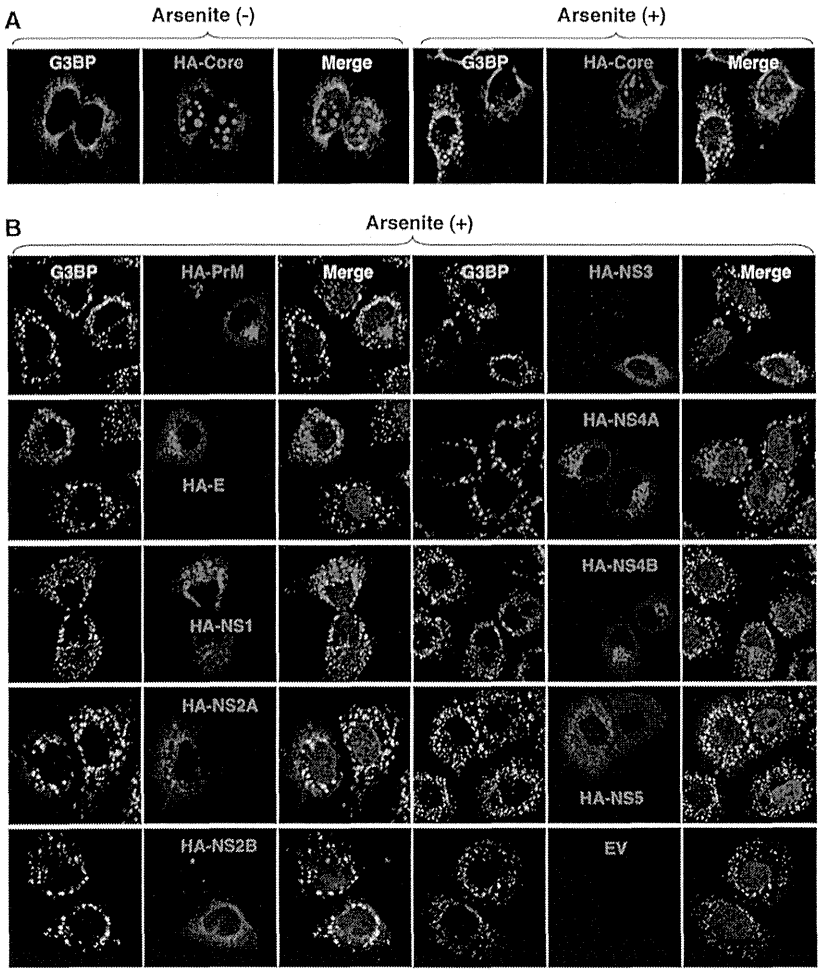

FIG 4 Inhibition of the arsenite-induced SG formation by the expression of JEV proteins. (A) Huh7 cells transfected with a plasmid, pCAGPM-HA-Core, were treated with or without 1.0 mM sodium arsenite for 30 min at 37°C, and the cellular localizations of G3BP and HA-Core were determined at 24 h posttransfection by immunofluorescence analysis with mouse anti-G3BP MAb and rat anti-HA MAb, followed by AF488-conjugated anti-mouse IgG and AF594-conjugated anti-rat IgG, respectively. Cell nuclei were stained with DAPI (blue). (B) Huh7 cells, which were separately transfected with a plasmid expressing an individual viral protein (pCAGPM-HA-JEV protein) as indicated in the figure, were treated with 1.0 mM sodium arsenite for 30 min at 37°C and subjected to an immunofluorescence assay using mouse anti-G3BP MAb and rat anti-HA MAb, followed by AF488-conjugated anti-mouse IgG and AF594-conjugated anti-rat IgG, respectively. Cell nuclei were stained with DAPI (blue).

formation induced by sodium arsenite, JEV-infected cells were treated with 0.5 mM sodium arsenite for 30 min at 24 h postinfection. Although many G3BP-positive foci were observed in mock-infected cells by the treatment with sodium arsenite, accumulation of G3BP in the perinuclear region was observed in the JEV-infected cells (Fig. 1A, right), and the numbers of G3BP-positive foci in the JEV-infected cells were less than those in the mock-infected cells (Fig. 1G). Although it has been reported that a significant reduction of the phosphorylation at Ser^{51} of eIF2α in cells treated with arsenite was induced by infection with WNV (15), the phosphorylation of eIF2α was slightly suppressed in the JEV-infected cells (Fig. 1C). Furthermore, while previous studies reported that Caprin-1 and TIA-1 were colocalized with dsRNA in cells infected with DENV (15, 26), no colocalization of G3BP or TIA-1 with the DENV core protein was observed in the present study (Fig. 3), suggesting that the mechanisms of the viral circumvention of SG formation in cells infected with JEV are different from those in cells infected with WNV and DENV.

JEV core protein suppresses SG formation induced by sodium arsenite. To elucidate the molecular mechanisms of suppression of SG formation induced by sodium arsenite during JEV infection, we tried to identify which viral protein(s) is responsible for the SG inhibition. Since G3BP was colocalized with JEV core protein, we first examined the involvement of the core protein in the perinuclear accumulation of G3BP and in the suppression of SG formation. The expression of JEV core protein alone induced the accumulation of G3BP in the perinuclear region (Fig. 4A, left panel) and suppressed sodium arsenite-induced SG formation (Fig. 4A, upper right cell in the right panel), similarly to JEV infection. In contrast, inhibition of SG formation induced by sodium arsenite was not observed in cells expressing other JEV proteins (Fig. 4B). These results suggest that JEV core protein is responsible for the circumvention of the SG formation observed in cells infected with JEV.

JEV core protein directly interacts with Caprin-1, an SG-associated cellular factor. Since JEV core protein was suggested to

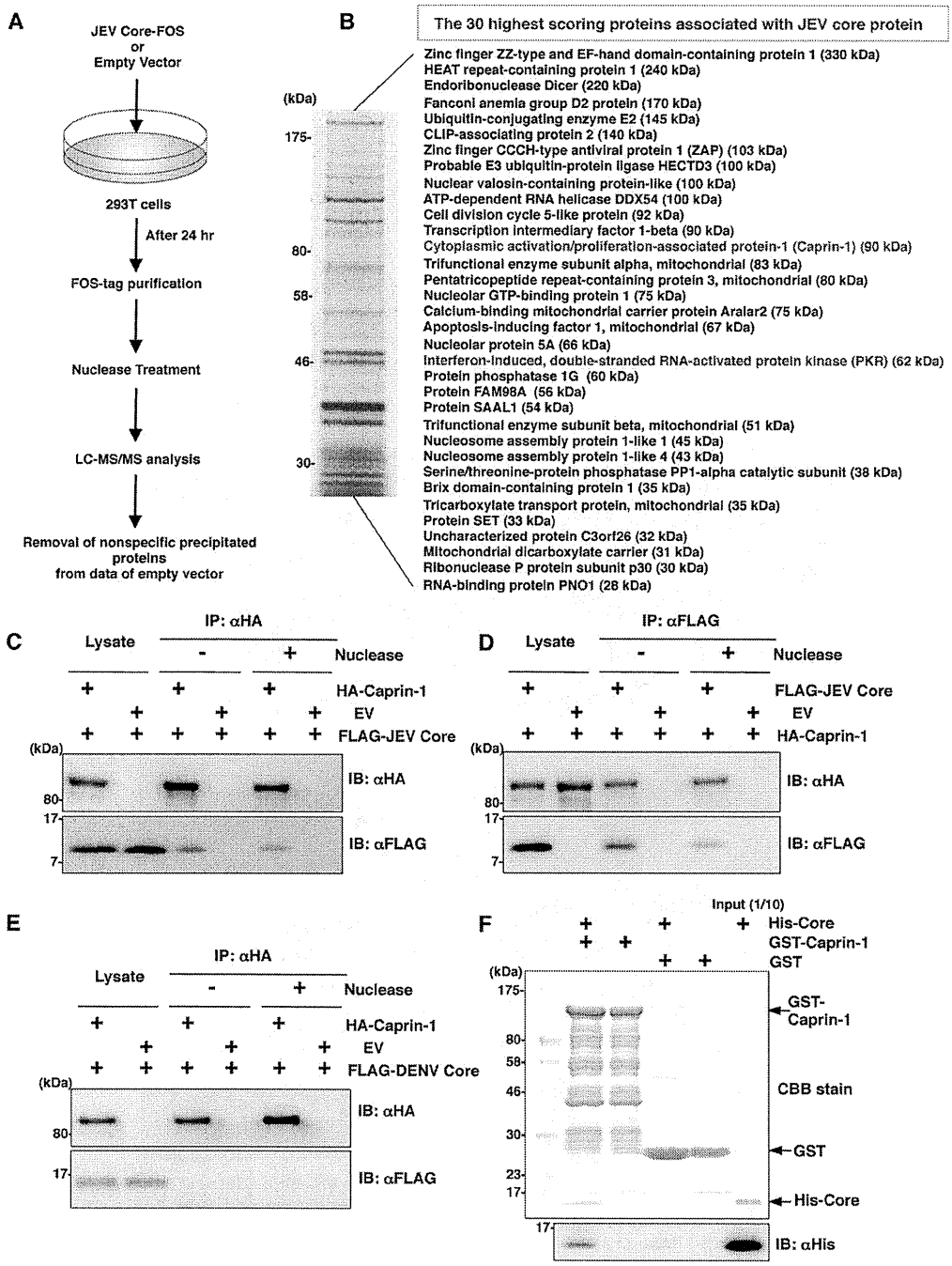

FIG 5 JEV core protein directly interacts with Caprin-1, an SG-associated cellular factor. (A) Identification of host cellular proteins associated with JEV core protein by FOS-tagged purification and LC-MS/MS analysis. Overview of the FOS-tagged purification of cellular proteins associated with JEV core protein. (B) The 30 candidate proteins as binding partners of JEV core protein exhibiting high scores are listed. PKR and Caprin-1 are indicated in red. (C and D) FLAG-JEV core protein and HA-Caprin-1 were coexpressed in 293T cells, and the cell lysates harvested at 24 h posttransfection were treated with or without micrococcal nuclease for 30 min at 37°C and immunoprecipitated (IP) with anti-HA (αHA) or anti-FLAG (αFLAG) antibody, as indicated. The precipitates were subjected to immunoblotting (IB) to detect coprecipitated counterparts. (E) FLAG-DENV core protein was coexpressed with HA-Caprin-1 in 293T cells, immunoprecipitated with anti-HA antibody, and immunoblotted with anti-HA or anti-FLAG antibody. (F) His-tagged JEV core protein was incubated with either GST-fused Caprin-1 or GST for 2 h at 4°C, and the precipitates obtained by GST pulldown assay were subjected to CBB staining and immunoblotting with anti-His antibody.

participate in the inhibition of SG formation, we tried to identify cellular factors associated with the core protein by LC-MS/MS analysis, as shown in Fig. 5A. Among the 30 factors with the best scores, two SG-associated proteins, PKR (Mascot search score, 206) and Caprin-1 (Mascot search score, 153), were identified as binding partners of JEV core protein (Fig. 5B). Although PABP1, hnRNP Q, Staufen, G3BP, and eIF4G were also identified, their scores were lower than those of PKR and Caprin-1. Because the

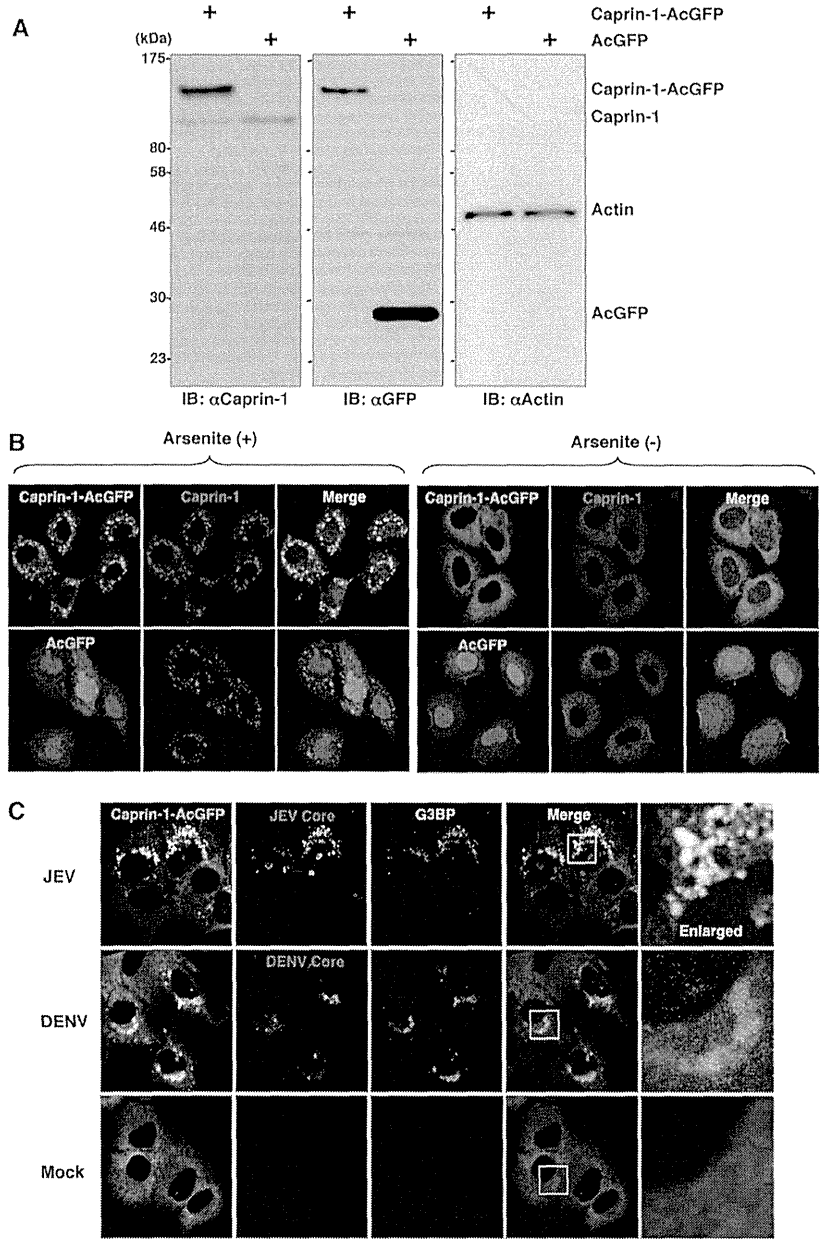

FIG 6 Caprin-1 is colocalized with the JEV core protein in the perinuclear region. (A) Expression of Caprin-1 fused with AcGFP (Caprin-1-AcGFP), Caprin-1, actin, or AcGFP in lentivirally transduced Huh7 cells was determined by immunoblotting using the appropriate antibodies. (B) Subcellular localization of Caprin-1-AcGFP or AcGFP (green) and endogenous Caprin-1 (red) in cells treated with/without 1.0 mM sodium arsenite for 30 min at 37°C was determined by immunofluorescence assay with rabbit anti-Caprin-1 PAb and AF594-conjugated anti-rabbit IgG. Cell nuclei were stained with DAPI (blue). (C) Huh7/Caprin-1-AcGFP cells were infected with either JEV or DENV at an MOI of 0.5, and the cellular localizations of JEV and DENV core (red) with Caprin-1-AcGFP and G3BP (blue) were determined at 24 h and 48 h postinfection, respectively. Cells were stained with mouse anti-G3BP MAb and rabbit anti-JEV or DENV core protein PAb, followed by AF633-conjugated anti-mouse IgG and AF594-conjugated anti-rabbit IgG, respectively, and examined by immunofluorescence analysis.

results shown in Fig. 1B suggest that the inhibition of SG formation takes place downstream of eIF2α phosphorylation, we focused on Caprin-1 as a key factor involved in the inhibition of SG formation in cells infected with JEV. To confirm the specific interaction of JEV core protein with Caprin-1, FLAG-JEV core protein and HA-Caprin-1 were coexpressed and immunoprecipitated with anti-HA or anti-FLAG antibody in the presence or absence of nuclease. FLAG-JEV core protein was coprecipitated with HA-Caprin-1 irrespective of nuclease treatment (Fig. 5C and D), suggesting that the interaction between JEV core protein and Caprin-1 is a protein-protein interaction. On the other hand, FLAG-DENV core protein was not coprecipitated with HA-Caprin-1 (Fig. 5E), indicating that the interaction with Caprin-1 was specific for JEV core protein. Next, the direct interaction be-

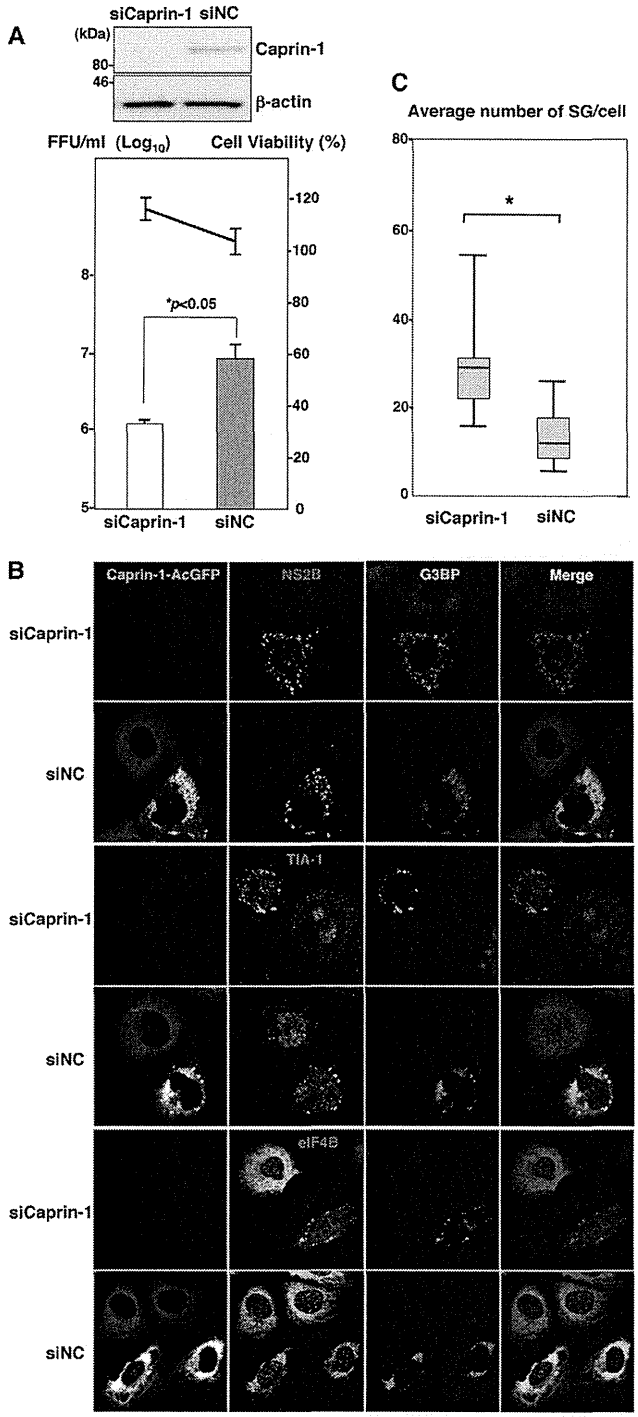

FIG 7 Knockdown of Caprin-1 cancels SG inhibition during JEV infection and suppresses viral propagation. (A) (Upper) The levels of expression of Caprin-1 in cells transfected with either siCaprin-1 or siNC was determined by immunoblotting using anti-Caprin-1 and anti-β-actin antibodies at 72 h posttransfection (top panel). At 48 h posttransfection with either siCaprin-1 or siNC, Huh7/Caprin-1-AcGFP cells were inoculated with JEV at an MOI of 0.5. At 24 h postinfection (72 h posttransfection), the infectious titers in the supernatants were determined by focus-forming assay in Vero cells (bottom panel, bar graph). Cell viability was determined at 72 h posttransfection and calculated as a percentage of the viability of cells treated with siNC (bottom panel, line graph). The results shown are from three independent assays, with the error bars representing the standard deviations. (B) At 48 h posttransfection with either siCaprin-1 or siNC, Huh7/Caprin-1-AcGFP cells were inoculated with JEV at an MOI of 0.5. The cellular localizations of SG-associated factors and JEV NS2B were determined at 24 h postinfection (72 h posttransfection) by immunofluorescence analysis with mouse anti-G3BP MAb and rabbit anti-NS2B PAb, rabbit anti-eIF4B PAb, or goat anti-TIA-1 PAb, followed by AF633-conjugated anti-mouse IgG and AF594-conjugated anti-rabbit IgG or AF594-conjugated anti-goat IgG, respectively. (C) Numbers of G3BP-positive foci in 30 cells prepared as described in panel B were counted. Lines, boxes, and error bars indicate the means, 25th to 75th percentiles, and 95th percentiles, respectively. The significance of differences between the means was determined by a Student's *t* test. *, $P < 0.01$.

tween JEV core protein and Caprin-1 was examined by a GST-pulldown assay using purified proteins expressed in bacteria. The His-tagged core protein was coprecipitated with GST-tagged Caprin-1, suggesting that JEV core protein directly interacts with Caprin-1 (Fig. 5F).

To further determine the cellular localization of Caprin-1 in JEV-infected cells, Caprin-1 fused with AcGFP (Caprin-1-AcGFP) was lentivirally expressed in Huh7 cells. The levels of expression and recruitment of Caprin-1-AcGFP into SGs were determined by immunoblotting and immunofluorescence analysis, respectively (Fig. 6A and B). In cells infected with JEV, Caprin-1-AcGFP was concentrated in the perinuclear region and colocalized with core protein and G3BP, while no colocalization of the proteins was observed in cells infected with DENV (Fig. 6C), suggesting that Caprin-1 directly interacts with JEV core protein in the perinuclear region of the infected cells.

Knockdown of Caprin-1 cancels SG inhibition during JEV infection and suppresses viral propagation. To assess the biological significance of the interaction of JEV core protein with Caprin-1 in JEV propagation, the expression of Caprin-1 was suppressed by using Caprin-1-specific siRNAs (siCaprin-1). Transfection of siCaprin-1 efficiently and specifically knocked down the expression of Caprin-1 with a slight increase of cell viability and decreased the production of infectious particles in the culture supernatants of cells infected with JEV, in comparison with those treated with a control siRNA (siNC) (Fig. 7A). Furthermore, immunofluorescence analyses revealed that knockdown of Caprin-1 increased the number of G3BP-positive granules colocalized with SG-associated factors, including TIA-1 and eIF4B, and inhibited the G3BP concentration in the perinuclear region (Fig. 7B and C). These results suggest that knockdown of Caprin-1 suppresses JEV propagation through the induction of SG formation.

Lys^{97} and Arg^{98} in the JEV core protein are crucial residues for the interaction with Caprin-1. To determine amino acid residues of the core protein that are required for the interaction with Caprin-1, we constructed a putative model based on the structural information of the DENV core protein previously resolved by nuclear magnetic resonance (NMR) (27), as shown in Fig. 8A. Based on this model, we selected hydrophobic amino acids, which were located on the solvent-exposed side in the α1 and α4 helices, as amino acid residues responsible for the binding to host proteins. Amino acid substitutions in each of the α-helices shown in Fig. 8B were designed in the context of FLAG-Core (Mα1 and Mα4), and the interaction of FLAG-Core mutants with Caprin-1 was examined by immunoprecipitation analysis. WT and Mα1, but not Mα4, core proteins were immunoprecipitated with Caprin-1 (Fig. 8B). To determine the amino acids responsible for interaction with Caprin-1, further alanine substitutions were introduced in the α4 helix, and the interaction was examined by immunopre-

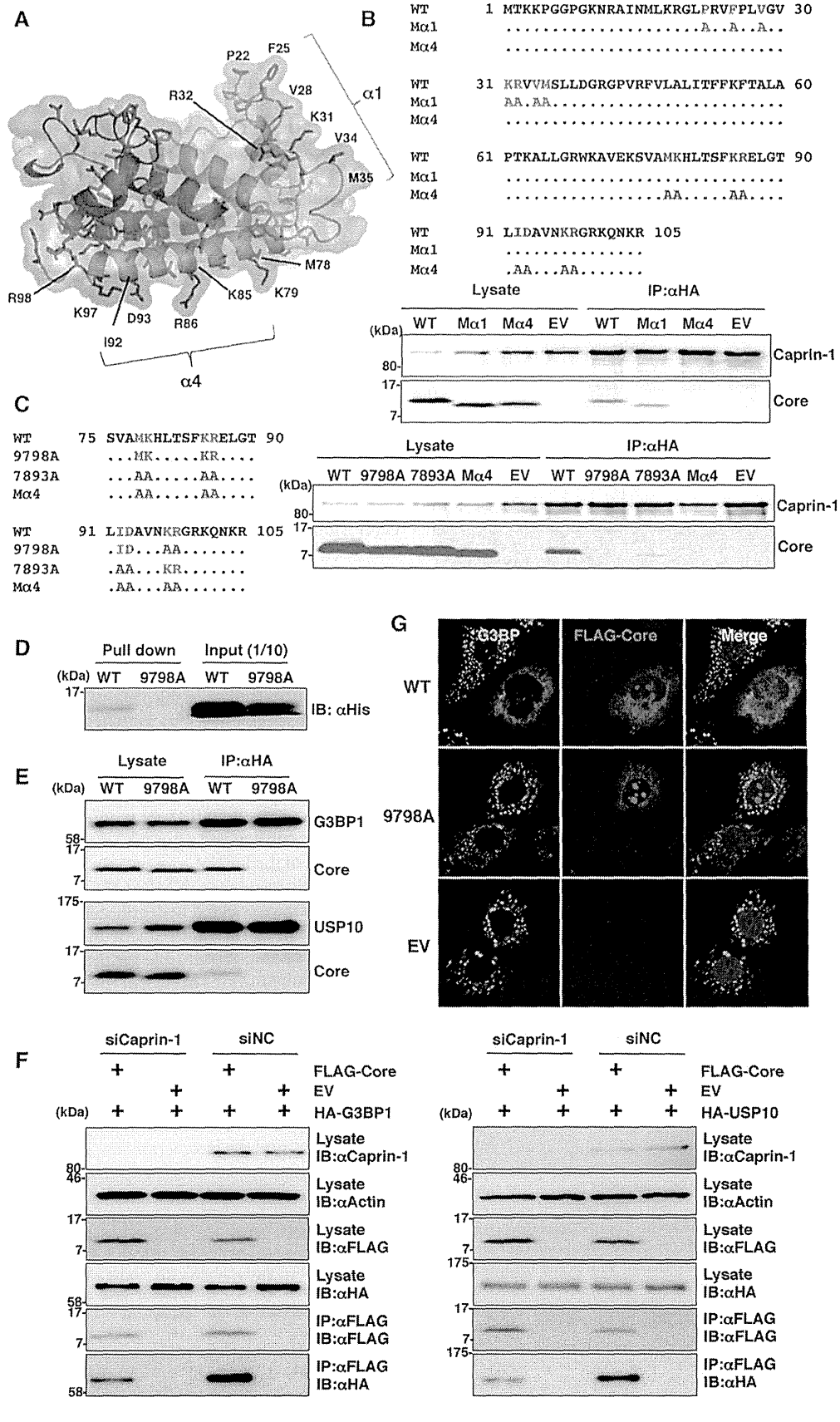
A
P22
F25
R32
V28
α1
K31
V34
M35
M78
R98
K97
D93
R86
K85
K79
I92
α4
B
WT 1 MTKKPGGPGKNRAINMLKRGLPRVFPLVGV 30
Mα1 .....A..A..A..
Mα4 .....
WT 31 KRVVMSLLDGRGPVRFVLALITFFKFTALA 60
Mα1 AA.AA.....
Mα4 .....
WT 61 PTKALLGRWKAVEKSVAMKHLTSFKRELGT 90
Mα1 .....
Mα4 .....AA.....AA....
WT 91 LIDAVNKRGRKQNKR 105
Mα1 .....
Mα4 .AA...AA.....
Lysate
IP:αHA
(kDa)
WT Mα1 Mα4 EV WT Mα1 Mα4 EV
80-
17-
7-
Caprin-1
Core
C
WT 75 SVAMKHLTSFKRELGT 90
9798A ...MK.....KR....
7893A ...AA.....AA....
Mα4 ...AA.....AA....
WT 91 LIDAVNKRGRKQNKR 105
9798A .ID...AA.....
7893A .AA...KR.....
Mα4 .AA...AA.....
Lysate
IP:αHA
(kDa)
WT 9798A 7893A Mα4 EV WT 9798A 7893A Mα4 EV
80-
17-
7-
Caprin-1
Core
D
Pull down
Input (1/10)
(kDa) WT 9798A WT 9798A
17-
IB: αHis
E
Lysate
IP:αHA
(kDa) WT 9798A WT 9798A
58-
17-
7-
175-
17-
7-
G3BP1
Core
USP10
Core
G
G3BP
FLAG-Core
Merge
WT
9798A
EV
F
siCaprin-1
siNC
siCaprin-1
siNC
+ + FLAG-Core
+ + EV
(kDa) + + + + HA-G3BP1
(kDa) + + + + HA-USP10
80-
46-
17-
7-
58-
17-
7-
58-
Lysate IB:αCaprin-1
Lysate IB:αActin
Lysate IB:αFLAG
Lysate IB:αHA
IP:αFLAG IB:αFLAG
IP:αFLAG IB:αHA
80-
46-
17-
7-
175-
17-
7-
175-
Lysate IB:αCaprin-1
Lysate IB:αActin
Lysate IB:αFLAG
Lysate IB:αHA
IP:αFLAG IB:αFLAG
IP:αFLAG IB:αHA

cipitation assay. As shown in Fig. 8C, double replacing both Lys^{97} and Arg^{98} with Ala (9798A) completely abrogated the interaction with Caprin-1. The importance of these two amino acids in the interaction with Caprin-1 was also confirmed by GST pulldown assay (Fig. 8D). These results indicate that Lys^{97} and Arg^{98} in the JEV core protein are crucial for the interaction with Caprin-1. Since G3BP has been reported to be one of the key molecules for SG formation and interacts with several SG component molecules including Caprin-1 and USP10 (28, 29), interactions of the core protein with SG components were examined by immunoprecipitation assay. The wild-type but not mutant 9798A core protein was associated with G3BP1 and USP10 (Fig. 8E). In addition, the knockdown of Caprin-1 weakened the interactions of core protein with G3BP1 or USP10 (Fig. 8F). These findings indicate that JEV core protein associates with several SG component molecules, such as G3BP1 and USP10, through the interaction with Caprin-1. Next, the role of the interaction between JEV core protein and Caprin-1 in the suppression of SG formation was examined by immunofluorescence analysis. Although the expression of the wild-type JEV core protein suppressed the SG formation induced by sodium arsenite treatment, as shown above, expression of the 9798A mutant did not (Fig. 8G), suggesting that the interaction of JEV core protein with Caprin-1 through Lys^{97} and Arg^{98} plays a crucial role in the inhibition of SG formation.

Interaction of the JEV core protein with Caprin-1 plays crucial roles not only in viral propagation *in vitro* but also in the pathogenesis in mice through the suppression of SG formation. To further examine the biological significance of the interaction between the JEV core protein and Caprin-1 in viral replication, we generated a mutant infectious cDNA clone (pMWJEAT/9798AA) of JEV encoding a mutant core protein deficient in the binding to Caprin-1 based on pMWJEAT. First, the cellular localization of the core protein in the 9798A mutant JEV-infected cells was examined by immunofluorescence analysis. The 9798A mutant core protein, as well as the wild-type core protein, was localized in the nucleus and the perinuclear region (Fig. 9A). However, the 9798A mutant core protein was not colocalized with Caprin-1, in contrast to the wild-type core protein. The sizes of infectious foci in Vero cells infected with the 9798A mutant were significantly smaller than those infected with the wild-type JEV (Fig. 9B). Furthermore, the infectious titers in C6/36 and Vero cells infected with the 9798A mutant were 6.1- and 12.6-fold lower than those infected with wild-type JEV at 48 h postinfection, respectively (Fig. 9C), suggesting that interaction of the JEV core protein with Caprin-1 plays crucial roles in the propagation of JEV in both insect and mammalian cells. Cells infected with the 9798A mutant induced SGs containing both G3BP and Caprin-1, in contrast to the accumulation of G3BP in the perinuclear region observed in those infected with the wild-type JEV (Fig. 9D). The numbers of foci in cells infected with the 9798A mutant were higher than those in cells infected with the wild-type JEV (Fig. 9E), indicating that the interaction of the JEV core protein with Caprin-1 is crucial for the suppression of SG formation. Finally, we examined the biological relevance of the interaction of JEV core protein with Caprin-1 in viral replication *in vivo*. Infectious particles were recovered from the cerebrums of ICR mice inoculated with wild-type JEV but not from those inoculated with the 9798A mutant (Fig. 9F). In addition, all 10 mice had died by 12 days postinoculation with the wild-type JEV, while only 1 mouse had died at day 10 postinoculation with the 9798A mutant (Fig. 9G). Collectively, these results suggest that the interaction of JEV core protein with Caprin-1 plays crucial roles not only in viral replication *in vitro* but also in pathogenesis in mice through the suppression of SG formation.

DISCUSSION

Viruses are obligatory intracellular parasites, and their life cycles rely on host cellular functions. Many viruses have evolved to inhibit SG formation and thereby evade the host translation shutoff mechanism and facilitate viral replication (6, 30), while some viruses co-opt molecules regulating SG formation for viral replication (11, 31). The vaccinia virus subverts SG components to generate aggregates containing G3BP, Caprin-1, eIF4G, eIF4E, and mRNA of the virus, but not of the host, in order to stimulate viral translation (11). Replication, translation, and assembly of transmissible gastroenteritis coronavirus, a member of the *Coronaviridae* family, are regulated by the interaction of polypyrimidine tract-binding protein and TIA-1 with viral RNA (31). HIV-1 utilizes Staufen1, which is a principal component of SG, in the viral RNA selection to form ribonucleoproteins (RNPs) through interaction with Gag protein, instead of SG translation silencing (8). In the case of flaviviruses, TIA-1 and TIAR bind to the 3′ untranslated region (UTR) of the negative-stranded RNA of WNV to facilitate viral replication (16), and G3BP1, Caprin-1, and USP10 interact with DENV RNA, although the biological significance of these interactions remains unknown (26). In this study, we have shown that JEV infection suppresses SG formation by the recruitment of several effector molecules promoting SG assembly, including G3BP and USP10, to the perinuclear region through the interaction of JEV core protein with Caprin-1. Furthermore, a mutant JEV carrying a core protein incapable of binding to

FIG 8 Lys^{97} and Arg^{98} in the JEV core protein are crucial residues for the interaction with Caprin-1. (A) Putative structural model of the core protein homodimer of JEV deduced from that of DENV obtained from the Protein Data Bank (accession number 1R6R) by using PyMOL software. The two α helices (α1 and α4) are indicated. (B) FLAG-Core mutants in which the hydrophobic amino acid residues in the α1 helix (Mα1) or α4 helix (Mα4) were replaced with alanine were coexpressed with HA-Caprin-1 in 293T cells, immunoprecipitated (IP) with anti-HA antibody, and examined by immunoblotting (IB) with anti-HA or anti-FLAG antibody. (C) FLAG-Core mutants in which the Met^{78}, Lys^{79}, Lys^{85}, Arg^{86}, Ile^{92}, and Asp^{93} (7893A) or Lys^{97} and Arg^{98} (9798A) in the α4 helix domain were replaced with alanine were coexpressed with HA-Caprin-1 in 293T cells and examined as described in panel B. (D) The His-tagged JEV core protein (WT or 9798A) was incubated with GST-fused Caprin-1 for 2 h at 4°C, and the precipitates obtained by GST pulldown assay were subjected to immunoblotting with anti-His antibody. (E) FLAG-Core (WT or 9798A) was coexpressed with HA-G3BP1 or HA-USP10 in 293T cells, immunoprecipitated with anti-HA antibody, and immunoblotted with anti-HA and anti-FLAG antibodies. (F) FLAG-JEV Core was coexpressed with HA-G3BP1 or HA-USP10 in 293T cells transfected with either siCaprin-1 or siNC at 72 h posttransfection, immunoprecipitated with anti-FLAG antibody, and immunoblotted with anti-HA and anti-FLAG antibodies. The cell lysates were also subjected to immunoblotting with anti-Caprin-1 and anti-β-actin antibodies to evaluate the knockdown efficiency of Caprin-1. (G) The cellular localizations of G3BP and FLAG-Core (WT or 9798A) were determined at 24 h posttransfection after treatment with 1.0 mM sodium arsenite for 30 min at 37°C by immunofluorescence analysis with mouse anti-G3BP MAb and rabbit anti-FLAG PAb, followed by AF488-conjugated anti-mouse IgG and AF594-conjugated anti-rabbit IgG, respectively. Cell nuclei were stained with DAPI (blue).

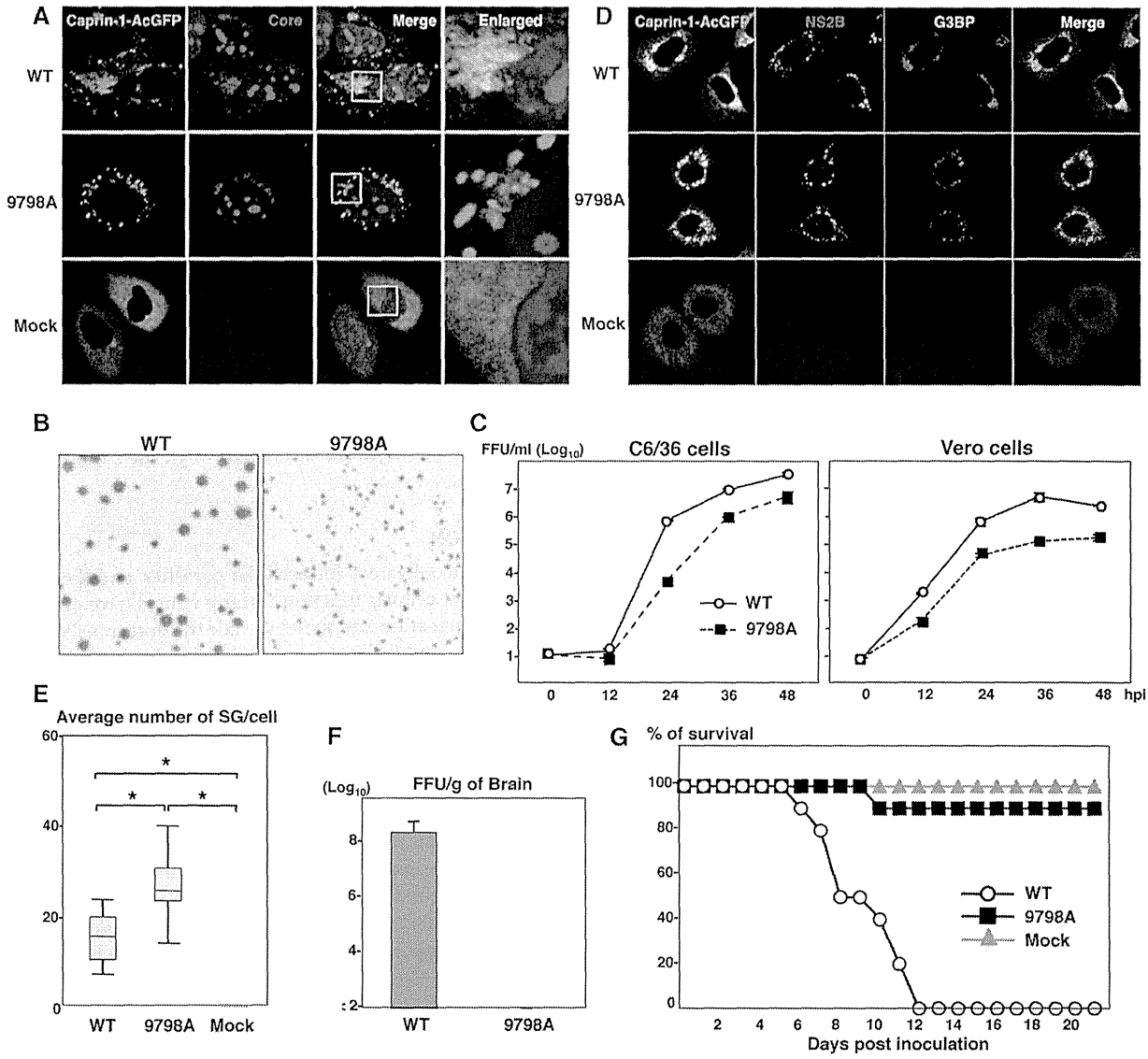

FIG 9 Interaction of JEV core protein with Caprin-1 plays crucial roles not only in viral replication *in vitro* but also in pathogenesis in mice through the suppression of SG formation. (A) Huh7/Caprin-1-AcGFP cells were infected with JEV (WT or 9798A mutant) at an MOI of 1.0, and the cellular localizations of Caprin-1-AcGFP and JEV core protein were determined at 24 h postinfection by immunofluorescence analysis with rabbit anti-core PAb and AF594-conjugated anti-rabbit IgG. Cell nuclei were stained with DAPI (blue). (B) Focus formation of JEV (WT or 9798A mutant) in Vero cells incubated in methylcellulose overlay medium at 48 h postinfection. The infectious foci were immunostained as described previously (20). (C) Growth kinetics of JEV (WT or 9798A mutant) in C6/36 and Vero cells infected at an MOI of 0.1. Infectious titers in the culture supernatants harvested at the indicated times were determined by focus-forming assays in Vero cells. Means of three experiments are indicated. (D) Huh7/Caprin-1-AcGFP cells were infected with either WT or 9798A at an MOI of 0.5, and cellular localizations of Caprin-1-AcGFP, G3BP (blue), and JEV NS2B (red) were determined at 24 h postinfection by immunofluorescence analysis with mouse anti-G3BP MAb and rabbit anti-NS2B PAb, followed by AF633-conjugated anti-mouse IgG and AF594-conjugated anti-rabbit IgG, respectively. (E) Numbers >of G3BP-positive foci in 30 cells prepared as described in panel D were counted. Lines, boxes, and error bars indicate the means, 25th to 75th percentiles, and 95th percentiles, respectively. The significance of differences between the means was determined by Student's *t* test. *, $P < 0.01$. (F) Infectious titers in the cerebrums of mice at 7 days postintraperitoneal inoculation with 5×10^4 FFU/100 μl of either WT or 9798A virus were determined in Vero cells. The means of titers in the homogenates of the cerebrums from three mice are indicated. The detection limit is 10^2 FFU/g of cerebrum. (G) Percentages of surviving mice ($n = 10$) after intraperitoneal inoculation with 5×10^4 FFU of either WT or 9798A virus. Mock, inoculation with DMEM.

Caprin-1 exhibited reduced replication *in vitro* and attenuated pathogenicity in mice.

G3BP is one of the key molecules involved in the SG aggregation process and self-oligomerizes in a phosphorylation-dependent manner to sequester mRNA in SGs (4). Therefore, G3BP knocked down cells (6) and G3BP knockout mouse embryonic fibroblast cells are deficient in the SG formation. In addition, G3BP sequestration inhibits SG formation in response to arsenite treatment (32). Caprin-1, known as RNA granule protein 105 or p137 (33), also participates in SG formation through phosphorylation of eIF2α (28) and is ubiquitously expressed in the cytoplasm. Caprin-1 regulates the transport and translation of mRNAs

of proteins involved in the synaptic plasticity in neurons (34) and cellular proliferation and migration in multiple cell types (28) through an interaction with G3BP. USP10, another SG-associated molecule, also interacts with G3BP and forms the G3BP/USP10 complex (29), suggesting that several SG-associated RBPs participate in the formation of a protein-protein network. In this study, the JEV core protein was shown to directly interact with Caprin-1, to sequester several key molecule complexes involved in SG formation to the perinuclear region in cells infected with JEV, and to facilitate viral propagation through the suppression of SG formation.

Flaviviruses replicate at a relatively low rate in comparison with most of the other positive-stranded RNA viruses, and thus rapid shutdown of host cellular protein synthesis would be deleterious for the viral life cycle. In cells infected with JEV, several SG components were colocalized with the core protein in the perinuclear region, while in those infected with WNV or DENV, SG components were accumulated in a replication complex composed of viral RNA and nonstructural proteins. In addition, the phosphorylation of eIF2α induced by arsenite was completely canceled by the infection with WNV or DENV, whereas the suppression of the phosphorylation was limited in JEV infection (15). Incorporation of the nascent viral RNA into the membranous structure induced by viral nonstructural proteins prevents PKR activation and inhibits SG formation in cells infected with WNV (17). In cells infected with hepatitis C virus (HCV), which belongs to the genus *Hepacivirus* in the family *Flaviviridae*, induction of SG formation was observed in the early stage of infection, in contrast to the inhibition of the arsenite-induced SG formation in the late stage (35). Several SG components, such as G3BP1, PABP1, and ataxin-2, were colocalized with HCV core protein around lipid droplets (35), and G3BP1 was also associated with the NS5B protein and the 5′ terminus of the minus-strand viral RNA (36) to mediate efficient viral replication. Collectively, these data suggest that flaviviruses have evolved to regulate cellular processes involved in SG formation through various strategies.

PKR is one of the interferon-stimulated genes and plays a crucial role in antiviral defense through phosphorylation of eIF2α, which leads to host translational shutoff (37, 38). In the early stage of flavivirus infection, both positive- and negative-stranded RNAs transcribe at low levels, while genomic RNA predominantly synthesizes in the late stage of infection (39). It was shown that activation of PKR was suppressed (40) or only induced in the late stage of WNV infection (41) and impaired by the expression of HCV NS5A (42–44). Very recently, JEV NS2A was shown to suppress PKR activation through inhibition of dimerization of PKR in the early stage but not in the late stage of infection (45). In this study, we have shown that JEV core protein interacts with Caprin-1 and inhibits SG formation downstream of the phosphorylation of eIF2α in the late stage of infection, suggesting that JEV has evolved to escape from host antiviral responses in the multiple stages of viral replication by using structural and nonstructural proteins.

The flavivirus core protein is a multifunctional protein involved in many aspects of the viral life cycle. In addition to the formation of viral nucleocapsid through the interaction with viral RNA (as a structural protein) (46), flavivirus core proteins interact with various host factors, such as B23 (47), Jab1 (48), hnRNP K (49), and hnRNP A2 (23), and regulate viral replication and/or modify the host cell environment (as a nonstructural protein). Although further investigations are needed to clarify the precise mechanisms underlying the circumvention of SG formation through the interaction of JEV core protein with Caprin-1, leading to efficient propagation *in vitro* and pathogenicity in mice, these findings could help not only to provide new insight into strategies by which viruses escape host stress responses but also to develop novel antiviral agents for flavivirus infection.

ACKNOWLEDGMENTS

We thank M. Tomiyama for secretarial assistance. We also thank K. Saito and T. Wakita for technical advice and the infectious clone of JEV, respectively.

This work was supported in part by grants-in-aid from the Ministry of Health, Labor, and Welfare, the Ministry of Education, Culture, Sports, Science, and Technology, and the Osaka University Global Center of Excellence Program. H. Katoh is a research fellow of the Japanese Society for the Promotion of Science.

REFERENCES

1. **Nover L, Scharf KD, Neumann D.** 1989. Cytoplasmic heat shock granules are formed from precursor particles and are associated with a specific set of mRNAs. Mol. Cell. Biol. **9**:1298–1308.
2. **Anderson P, Kedersha N.** 2002. Stressful initiations. J. Cell Sci. **115**:3227–3234.
3. **Gilks N, Kedersha N, Ayodele M, Shen L, Stoecklin G, Dember LM, Anderson P.** 2004. Stress granule assembly is mediated by prion-like aggregation of TIA-1. Mol. Biol. Cell **15**:5383–5398.
4. **Tourriere H, Chebli K, Zekri L, Courselaud B, Blanchard JM, Bertrand E, Tazi J.** 2003. The RasGAP-associated endoribonuclease G3BP assembles stress granules. J. Cell Biol. **160**:823–831.
5. **Kedersha N, Cho MR, Li W, Yacono PW, Chen S, Gilks N, Golan DE, Anderson P.** 2000. Dynamic shuttling of TIA-1 accompanies the recruitment of mRNA to mammalian stress granules. J. Cell Biol. **151**:1257–1268.
6. **White JP, Cardenas AM, Marissen WE, Lloyd RE.** 2007. Inhibition of cytoplasmic mRNA stress granule formation by a viral proteinase. Cell Host Microbe **2**:295–305.
7. **Khaperskyy DA, Hatchette TF, McCormick C.** 2012. Influenza A virus inhibits cytoplasmic stress granule formation. FASEB J. **26**:1629–1639.
8. **Abrahamyan LG, Chatel-Chaix L, Ajamian L, Milev MP, Monette A, Clement JF, Song R, Lehmann M, DesGroseillers L, Laughrea M, Boccaccio G, Mouland AJ.** 2010. Novel Staufen1 ribonucleoproteins prevent formation of stress granules but favour encapsidation of HIV-1 genomic RNA. J. Cell Sci. **123**:369–383.
9. **McInerney GM, Kedersha NL, Kaufman RJ, Anderson P, Liljestrom P.** 2005. Importance of eIF2α phosphorylation and stress granule assembly in alphavirus translation regulation. Mol. Biol. Cell **16**:3753–3763.
10. **Smith JA, Schmechel SC, Raghavan A, Abelson M, Reilly C, Katze MG, Kaufman RJ, Bohjanen PR, Schiff LA.** 2006. Reovirus induces and benefits from an integrated cellular stress response. J. Virol. **80**:2019–2033.
11. **Katsafanas GC, Moss B.** 2007. Colocalization of transcription and translation within cytoplasmic poxvirus factories coordinates viral expression and subjugates host functions. Cell Host Microbe **2**:221–228.
12. **Misra UK, Kalita J.** 2010. Overview: Japanese encephalitis. Prog. Neurobiol. **91**:108–120.
13. **Sumiyoshi H, Mori C, Fuke I, Morita K, Kuhara S, Kondou J, Kikuchi Y, Nagamatu H, Igarashi A.** 1987. Complete nucleotide sequence of the Japanese encephalitis virus genome RNA. Virology **161**:497–510.
14. **Murray CL, Jones CT, Rice CM.** 2008. Architects of assembly: roles of *Flaviviridae* non-structural proteins in virion morphogenesis. Nat. Rev. Microbiol. **6**:699–708.
15. **Emara MM, Brinton MA.** 2007. Interaction of TIA-1/TIAR with West Nile and dengue virus products in infected cells interferes with stress granule formation and processing body assembly. Proc. Natl. Acad. Sci. U. S. A. **104**:9041–9046.
16. **Li W, Li Y, Kedersha N, Anderson P, Emara M, Swiderek KM, Moreno GT, Brinton MA.** 2002. Cell proteins TIA-1 and TIAR interact with the 3′ stem-loop of the West Nile virus complementary minus-strand RNA and facilitate virus replication. J. Virol. **76**:11989–12000.
17. **Courtney SC, Scherbik SV, Stockman BM, Brinton MA.** 2012. West Nile

virus infections suppress early viral RNA synthesis and avoid inducing the cell stress granule response. J. Virol. 86:3647–3657.
18. Kambara H, Tani H, Mori Y, Abe T, Katoh H, Fukuhara T, Taguwa S, Moriishi K, Matsuura Y. 2011. Involvement of cyclophilin B in the replication of Japanese encephalitis virus. Virology 412:211–219.
19. Mori Y, Yamashita T, Tanaka Y, Tsuda Y, Abe T, Moriishi K, Matsuura Y. 2007. Processing of capsid protein by cathepsin L plays a crucial role in replication of Japanese encephalitis virus in neural and macrophage cells. J. Virol. 81:8477–8487.
20. Mori Y, Okabayashi T, Yamashita T, Zhao Z, Wakita T, Yasui K, Hasebe F, Tadano M, Konishi E, Moriishi K, Matsuura Y. 2005. Nuclear localization of Japanese encephalitis virus core protein enhances viral replication. J. Virol. 79:3448–3458.
21. Kambara H, Fukuhara T, Shiokawa M, Ono C, Ohara Y, Kamitani W, Matsuura Y. 2012. Establishment of a novel permissive cell line for the propagation of hepatitis C virus by expression of microRNA miR122. J. Virol. 86:1382–1393.
22. Zhao Z, Date T, Li Y, Kato T, Miyamoto M, Yasui K, Wakita T. 2005. Characterization of the E-138 (Glu/Lys) mutation in Japanese encephalitis virus by using a stable, full-length, infectious cDNA clone. J. Gen. Virol. 86:2209–2220.
23. Katoh H, Mori Y, Kambara H, Abe T, Fukuhara T, Morita E, Moriishi K, Kamitani W, Matsuura Y. 2011. Heterogeneous nuclear ribonucleoprotein A2 participates in the replication of Japanese encephalitis virus through an interaction with viral proteins and RNA. J. Virol. 85:10976–10988.
24. Hamamoto I, Nishimura Y, Okamoto T, Aizaki H, Liu M, Mori Y, Abe T, Suzuki T, Lai MM, Miyamura T, Moriishi K, Matsuura Y. 2005. Human VAP-B is involved in hepatitis C virus replication through interaction with NS5A and NS5B. J. Virol. 79:13473–13482.
25. Jones CT, Ma L, Burgner JW, Groesch TD, Post CB, Kuhn RJ. 2003. Flavivirus capsid is a dimeric alpha-helical protein. J. Virol. 77:7143–7149.
26. Ward AM, Bidet K, Yinglin A, Ler SG, Hogue K, Blackstock W, Gunaratne J, Garcia-Blanco MA. 2011. Quantitative mass spectrometry of DENV-2 RNA-interacting proteins reveals that the DEAD-box RNA helicase DDX6 binds the DB1 and DB2 3′ UTR structures. RNA Biol. 8:1173–1186.
27. Ma L, Jones CT, Groesch TD, Kuhn RJ, Post CB. 2004. Solution structure of dengue virus capsid protein reveals another fold. Proc. Natl. Acad. Sci. U. S. A. 101:3414–3419.
28. Solomon S, Xu Y, Wang B, David MD, Schubert P, Kennedy D, Schrader JW. 2007. Distinct structural features of Caprin-1 mediate its interaction with G3BP-1 and its induction of phosphorylation of eukaryotic translation initiation factor 2α, entry to cytoplasmic stress granules, and selective interaction with a subset of mRNAs. Mol. Cell. Biol. 27:2324–2342.
29. Soncini C, Berdo I, Draetta G. 2001. Ras-GAP SH3 domain binding protein (G3BP) is a modulator of USP10, a novel human ubiquitin specific protease. Oncogene 20:3869–3879.
30. Montero H, Rojas M, Arias CF, Lopez S. 2008. Rotavirus infection induces the phosphorylation of eIF2α but prevents the formation of stress granules. J. Virol. 82:1496–1504.
31. Sola I, Galan C, Mateos-Gomez PA, Palacio L, Zuniga S, Cruz JL, Almazan F, Enjuanes L. 2011. The polypyrimidine tract-binding protein affects coronavirus RNA accumulation levels and relocalizes viral RNAs to novel cytoplasmic domains different from replication-transcription sites. J. Virol. 85:5136–5149.
32. Hinton SD, Myers MP, Roggero VR, Allison LA, Tonks NK. 2010. The pseudophosphatase MK-STYX interacts with G3BP and decreases stress granule formation. Biochem. J. 427:349–357.
33. Grill B, Wilson GM, Zhang KX, Wang B, Doyonnas R, Quadroni M, Schrader JW. 2004. Activation/division of lymphocytes results in increased levels of cytoplasmic activation/proliferation-associated protein-1: prototype of a new family of proteins. J. Immunol. 172:2389–2400.
34. Shiina N, Shinkura K, Tokunaga M. 2005. A novel RNA-binding protein in neuronal RNA granules: regulatory machinery for local translation. J. Neurosci. 25:4420–4434.
35. Ariumi Y, Kuroki M, Kushima Y, Osugi K, Hijikata M, Maki M, Ikeda M, Kato N. 2011. Hepatitis C virus hijacks P-body and stress granule components around lipid droplets. J. Virol. 85:6882–6892.
36. Yi Z, Pan T, Wu X, Song W, Wang S, Xu Y, Rice CM, Macdonald MR, Yuan Z. 2011. Hepatitis C virus co-opts Ras-GTPase-activating protein-binding protein 1 for its genome replication. J. Virol. 85:6996–7004.
37. Gale M, Jr, Katze MG. 1998. Molecular mechanisms of interferon resistance mediated by viral-directed inhibition of PKR, the interferon-induced protein kinase. Pharmacol. Ther. 78:29–46.
38. Pindel A, Sadler A. 2011. The role of protein kinase R in the interferon response. J. Interferon Cytokine Res. 31:59–70.
39. Chu PW, Westaway EG. 1985. Replication strategy of Kunjin virus: evidence for recycling role of replicative form RNA as template in semiconservative and asymmetric replication. Virology 140:68–79.
40. Elbahesh H, Scherbik SV, Brinton MA. 2011. West Nile virus infection does not induce PKR activation in rodent cells. Virology 421:51–60.
41. Samuel MA, Whitby K, Keller BC, Marri A, Barchet W, Williams BR, Silverman RH, Gale M, Jr, Diamond MS. 2006. PKR and RNase L contribute to protection against lethal West Nile Virus infection by controlling early viral spread in the periphery and replication in neurons. J. Virol. 80:7009–7019.
42. Gale M, Jr, Blakely CM, Kwieciszewski B, Tan SL, Dossett M, Tang NM, Korth MJ, Polyak SJ, Gretch DR, Katze MG. 1998. Control of PKR protein kinase by hepatitis C virus nonstructural 5A protein: molecular mechanisms of kinase regulation. Mol. Cell. Biol. 18:5208–5218.
43. Gale MJ, Jr, Korth MJ, Tang NM, Tan SL, Hopkins DA, Dever TE, Polyak SJ, Gretch DR, Katze MG. 1997. Evidence that hepatitis C virus resistance to interferon is mediated through repression of the PKR protein kinase by the nonstructural 5A protein. Virology 230:217–227.
44. He Y, Tan SL, Tareen SU, Vijaysri S, Langland JO, Jacobs BL, Katze MG. 2001. Regulation of mRNA translation and cellular signaling by hepatitis C virus nonstructural protein NS5A. J. Virol. 75:5090–5098.
45. Tu YC, Yu CY, Liang JJ, Lin E, Liao CL, Lin YL. 2012. Blocking dsRNA-activated protein kinase PKR by Japanese encephalitis virus nonstructural protein 2A. J. Virol. 86:10347–10358.
46. Khromykh AA, Westaway EG. 1996. RNA binding properties of core protein of the flavivirus Kunjin. Arch. Virol. 141:685–699.
47. Tsuda Y, Mori Y, Abe T, Yamashita T, Okamoto T, Ichimura T, Moriishi K, Matsuura Y. 2006. Nucleolar protein B23 interacts with Japanese encephalitis virus core protein and participates in viral replication. Microbiol. Immunol. 50:225–234.
48. Oh W, Yang MR, Lee EW, Park KM, Pyo S, Yang JS, Lee HW, Song J. 2006. Jab1 mediates cytoplasmic localization and degradation of West Nile virus capsid protein. J. Biol. Chem. 281:30166–30174.
49. Chang CJ, Luh HW, Wang SH, Lin HJ, Lee SC, Hu ST. 2001. The heterogeneous nuclear ribonucleoprotein K (hnRNP K) interacts with dengue virus core protein. DNA Cell Biol. 20:569–577.

Molecular Biology | Virology | Cell Biology

BioTechniques Rapid Dispatches

Benchmarks

Attenuated protein expression vectors for use in siRNA rescue experiments

Eiji Morita*, Jun Arii*, Devin Christensen, Jörg Votteler, and Wesley I. Sundquist
Department of Biochemistry, University of Utah School of Medicine, Salt Lake City, UT, USA

*E.M. and J.A. contributed equally

Transient transfection of small interfering RNA (siRNA) provides a powerful approach for studying cellular protein functions, particularly when the target protein can be re-expressed from an exogenous siRNA-resistant construct in order to rescue the knockdown phenotype, confirm siRNA target specificity, and support mutational analyses. Rescue experiments often fail, however, when siRNA-resistant constructs are expressed at suboptimal levels. Here, we describe an ensemble of mammalian protein expression vectors with CMV promoters of differing strengths. Using CHMP2A rescue of HIV-1 budding, we show that these vectors can combine high-transfection efficiencies with tunable protein expression levels to optimize the rescue of cellular phenotypes induced by siRNA transfection.

Keywords: siRNA; CMV promoter; mammalian protein expression; phenotypic rescue; HIV-1 budding; ESCRT; CHMP2

Small interfering RNAs (siRNAs) are commonly employed, both individually and on a genome-wide scale, to degrade specific mRNAs and test the cellular requirements for their encoded proteins (1–7). The basic siRNA depletion experiment can be extended further using "rescue" experiments in which the target protein is re-expressed from a transiently transfected vector that encodes an altered mRNA resistant to siRNA silencing (8–10). This experiment is useful for confirming siRNA specificity because the exogenously expressed protein should rescue the loss-of-function phenotype. The experiment also enables genetic analyses in cultured mammalian cells because the functional effects of specific mutations can be tested. Phenotypic rescue experiments can fail, however, when the rescuing protein is expressed at such a high level that it dominantly inhibits the pathway of interest. This problem can often be alleviated by reducing the quantity of transfected expression vector, but this approach fails if the overall transfection efficiency is reduced. To address this problem, we created an ensemble of seven mammalian expression vectors designed to allow more precise control of exogenous protein expression levels. These vectors have nested deletions that successively eliminate transcription factor binding sites within the human cytomegalovirus (CMV) intermediate early enhancer/promoter (summarized in Figure 1 and Supplemental Table 1, and see Supplemental Figure 1 for promoter DNA sequences and a summary of the design strategy). The deletions were made in the context of the mammalian expression vector pcDNA3.1/myc-His(-)A, that contained a custom-designed multiple cloning site (MCS) cassette. These vectors allow optimized expression of siRNA-resistant constructs, while maintaining the high transfection efficiencies necessary for potent phenotypic rescue.

HIV-1 and many other enveloped viruses recruit the cellular endosomal sorting complexes required for transport (ESCRT) pathway to facilitate the final membrane fission step of virus budding (11–14). As is true for many other cellular pathways, siRNA depletion/rescue experiments have contributed to our understanding of the role of the ESCRT pathway in HIV-1 budding (9,15). We have found, however, that it is often difficult to rescue virus budding to wild type levels following siRNA depletion because many ESCRT proteins, particularly those of the ESCRT-III family, can potently inhibit HIV-1 budding when overexpressed at elevated levels (16–20). The ESCRT-III/HIV-1 system therefore represents an attractive test case for examining the utility of our family of attenuated CMV expression vectors.

HIV-1 budding from cultured 293T cells can be potently inhibited by co-depletion of both members of the human CHMP2 family of ESCRT-III proteins (denoted CHMP2A and CHMP2B) (15). Hence, vector titers were dramatically reduced 48 h after co-transfection of a proviral HIV-1 vector together with siRNAs that targeted both CHMP2 proteins (Figure 2A, 24 ± 5-fold reduction, compare lanes 1 and 2). CHMP2 depletion also blocked virus release into the culture supernatant, as measured by immunoblotting for the virion-associated structural proteins, MA and CA (Figure 2A, panel

Method summary:

We have created a family of mammalian protein expression vectors with cytomegalovirus promoters of differing strengths and shown that these vectors can combine high-transfection efficiencies with tunable protein expression levels to optimize the rescue of cellular phenotypes induced by siRNA transfection.

2, compare lanes 1 and 2). Western blots of the 293T producing cells demonstrated that both CHMP2A and CHMP2B were depleted efficiently (Figure 2A, panels 4 and 5, compare lanes 1 and 2) and that cellular levels of the structural HIV-1 Gag protein and its MA and CA cleavage products were not altered significantly by CHMP2 protein depletion (Figure 2A, panel 3, compare lanes 1 and 2).

To test for rescue of virus budding, 500 ng of each of the different siRNA-resistant pCMV-CHMP2A expression vectors were co-transfected together with the siRNA and proviral HIV-1 (Figure 2A). As expected, CHMP2A expression levels were highest for the construct that carried the wild type CMV promoter (denoted pCMV(WT)-CHMP2A) and decreased successively over two orders of magnitude as larger and larger promoter deletions were introduced (denoted pCMV(Δ1)-CHMP2A to pCMV(Δ7)-CHMP2A, (Figure 2A, panel 4, compare lanes 3–10)). In contrast, the rescue of virus budding was biphasic: virion release and infectivity were low when CHMP2A levels were highest, increased when CHMP2A was expressed at intermediate levels, and then decreased again at the lowest CHMP2A expression levels (Figure 2A, panels 1 and 2, compare lanes 3–10). Levels of virion release and infectivity generally correlated well, but maximal infectivity occurred at slightly higher CHMP2A levels, perhaps because rapid virus release kinetics contribute more to viral infectivity than to total virion release as measured in the end point release assay. The pCMV(Δ4)-CHMP2A and pCMV(Δ5)-CHMP2A constructs expressed CHMP2A at levels that most closely approximated the normal level of the endogenous protein (Figure 2A, panel 4, compare lanes 7 and 8 to lane 1). These two CHMP2A expression constructs also rescued virus release and infectivity best (Figure 2A, panels 1 and 2). Importantly, the pCMV(Δ4)-CHMP2A construct rescued viral titers very efficiently, to 102 ± 12% of untreated control levels. These data imply that: *(i)* CHMP2A alone can fully rescue HIV-1 budding, even in the absence of CHMP2B; *(ii)* CHMP2A functions best when expressed at near-native levels; and *(iii)* the attenuated pCMV(Δ4)-CHMP2A and pCMV(Δ5)-CHMP2A constructs can express near-native levels of CHMP2A under conditions where transfection efficiencies apparently remain high.

We next tested whether HIV-1 budding could be rescued to comparable levels simply by varying the quantity of pCMV(WT)-CHMP2A used in the transfection reaction. 3-fold dilutions over a range of 500–0.69 ng of pCMV(WT)-CHMP2A were tested for rescue of HIV-1 budding from cells that lacked endogenous CHMP2 proteins. CHMP2A expression levels correlated well with the quantity of pCMV(WT)-CHMP2A vector used (Figure 2B, panel 4, lanes 3–9), and CHMP2A levels most closely approximated normal endogenous protein levels when 56 and 19 ng of pCMV(WT)-CHMP2A were used (compare lane 1 to lanes 6 and 7). Rescue of HIV-1 budding again followed a biphasic curve, with optimal rescue observed when CHMP2A was expressed at intermediate levels (170–19 ng pCMV(WT)-CHMP2A, lanes 5–7). In this case, however, HIV-1 titers never exceeded 26% of control levels, even when the bulk levels of exogenous CHMP2A approximated endogenous control levels (Figure 2B, panel 1, compare lane 1 to lanes 6 and 7). In a parallel control experiment, HIV-1 release was again rescued to nearly wild type levels upon co-transfection of 500 ng of the pCMV(Δ4)-CHMP2A construct (lane 10). We therefore conclude that although optimizing pCMV(WT)-CHMP2A vector levels improved HIV-1 budding, overall rescue levels were never as high as could be achieved with the attenuated pCMV(Δ4)-CHMP2 expression construct.

We hypothesized that the pCMV(Δ4)-CHMP2A and pCMV(Δ5)-CHMP2A vectors worked well in the rescue experiment because they could be used at concentrations that coupled high transfection efficiencies with restricted protein expression. To test this idea, we created pCMV(WT)-YFP, pCMV(Δ4)-YFP and pCMV(Δ5)-YFP expression vectors and used YFP fluorescence as a measure of protein expression in 293T cells. This approach allowed us to use flow cytometry to quantify transfection efficiencies and relative protein expression levels at the single-cell level. Titrations were again performed to determine the quantity of pCMV(WT)-YFP required to express YFP at levels comparable to those produced by transfections with 500 ng of pCMV(Δ4)-YFP or pCMV(Δ5)-YFP. This was achieved with 19 ng of pCMV(WT)-YFP, in reasonable agreement with the analogous CHMP2A titration experiments (Figure 3A, compare total mean fluorescence levels for 500 ng of pCMV(Δ4)-YFP or pCMV(Δ5)-YFP DNA with 19 ng of pCMV(WT)-YFP). As shown in Figure 3B, overall transfection efficiencies under these three conditions were: 94 ± 1% for 500 ng of pCMV(Δ4)-YFP, 90 ± 2% for 500 ng of pCMV(Δ5)-YFP DNA and 36 ± 8% for 19 ng pCMV(WT)-YFP (compare lanes 2, 3 and 5). Thus, overall transfection efficiencies dropped off significantly when the quantity of vector was reduced from 500 to 19 ng. We also quantified the mean fluorescence intensity (MFI) in the subsets of cells that were actually transfected in each reaction (i.e., now excluding cells in which YFP expression was undetectable). As shown in Figure 3C, transfected cells in the 19 ng pCMV(WT)-YFP reaction had a MFI of

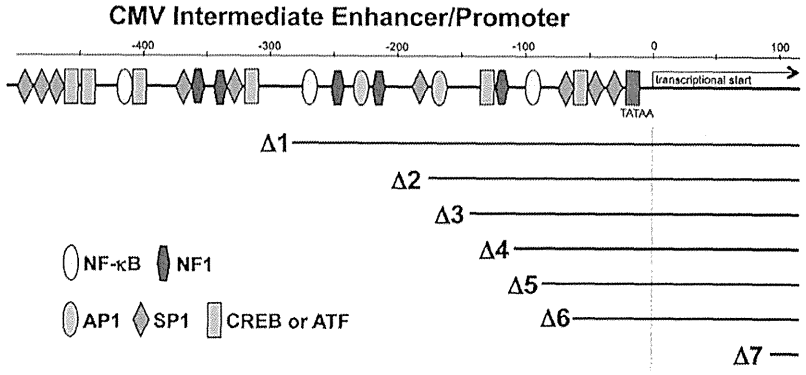

Figure 1. Human cytomegalovirus major immediate early enhancer/promoter constructs used for attenuated gene expression. The human CMV promoter structure is shown above, with the transcription start site at the +1 position and (putative) upstream binding sites for different transcription factors. Promoter deletion positions are shown below. Transcription factor binding elements were identified using the TESS analysis tool (22), with a consensus sequence cutoff of >12.0. Similar but slightly different variants of this binding site map were also generated by the program TFSEARCH (23) and have been published (24). Promoter deletions were introduced by cloning PCR fragments (*MluI*-*XbaI* sites) with the designated deletions into a pcDNA 3.1/myc-His(-)A expression vector (Life Technologies) that carried a custom multicloning site between the *XbaI* and *AflII* sites. Deletion design and DNA sequences are provided in Supplementary Figure 1, and construct numbers are provided in Supplementary Table 1.

2, compare lanes 1 and 2). Western blots of the 293T producing cells demonstrated that both CHMP2A and CHMP2B were depleted efficiently (Figure 2A, panels 4 and 5, compare lanes 1 and 2) and that cellular levels of the structural HIV-1 Gag protein and its MA and CA cleavage products were not altered significantly by CHMP2 protein depletion (Figure 2A, panel 3, compare lanes 1 and 2).

To test for rescue of virus budding, 500 ng of each of the different siRNA-resistant pCMV-CHMP2A expression vectors were co-transfected together with the siRNA and proviral HIV-1 (Figure 2A). As expected, CHMP2A expression levels were highest for the construct that carried the wild type CMV promoter (denoted pCMV(WT)-CHMP2A) and decreased successively over two orders of magnitude as larger and larger promoter deletions were introduced (denoted pCMV(Δ1)-CHMP2A to pCMV(Δ7)-CHMP2A, (Figure 2A, panel 4, compare lanes 3–10)). In contrast, the rescue of virus budding was biphasic: virion release and infectivity were low when CHMP2A levels were highest, increased when CHMP2A was expressed at intermediate levels, and then decreased again at the lowest CHMP2A expression levels (Figure 2A, panels 1 and 2, compare lanes 3–10). Levels of virion release and infectivity generally correlated well, but maximal infectivity occurred at slightly higher CHMP2A levels, perhaps because rapid virus release kinetics contribute more to viral infectivity than to total virion release as measured in the end point release assay. The pCMV(Δ4)-CHMP2A and pCMV(Δ5)-CHMP2A constructs expressed CHMP2A at levels that most closely approximated the normal level of the endogenous protein (Figure 2A, panel 4, compare lanes 7 and 8 to lane 1). These two CHMP2A expression constructs also rescued virus release and infectivity best (Figure 2A, panels 1 and 2). Importantly, the pCMV(Δ4)-CHMP2A construct rescued viral titers very efficiently, to 102 ± 12% of untreated control levels. These data imply that: *(i)* CHMP2A alone can fully rescue HIV-1 budding, even in the absence of CHMP2B; *(ii)* CHMP2A functions best when expressed at near-native levels; and *(iii)* the attenuated pCMV(Δ4)-CHMP2A and pCMV(Δ5)-CHMP2A constructs can express near-native levels of CHMP2A under conditions where transfection efficiencies apparently remain high.

We next tested whether HIV-1 budding could be rescued to comparable levels simply by varying the quantity of pCMV(WT)-CHMP2A used in the transfection reaction. 3-fold dilutions over a range of 500–0.69 ng of pCMV(WT)-CHMP2A were tested for rescue of HIV-1 budding from cells that lacked endogenous CHMP2 proteins. CHMP2A expression levels correlated well with the quantity of pCMV(WT)-CHMP2A vector used (Figure 2B, panel 4, lanes 3–9), and CHMP2A levels most closely approximated normal endogenous protein levels when 56 and 19 ng of pCMV(WT)-CHMP2A were used (compare lane 1 to lanes 6 and 7). Rescue of HIV-1 budding again followed a biphasic curve, with optimal rescue observed when CHMP2A was expressed at intermediate levels (170–19 ng pCMV(WT)-CHMP2A, lanes 5–7). In this case, however, HIV-1 titers never exceeded 26% of control levels, even when the bulk levels of exogenous CHMP2A approximated endogenous control levels (Figure 2B, panel 1, compare lane 1 to lanes 6 and 7). In a parallel control experiment, HIV-1 release was again rescued to nearly wild type levels upon co-transfection of 500 ng of the pCMV(Δ4)-CHMP2A construct (lane 10). We therefore conclude that although optimizing pCMV(WT)-CHMP2A vector levels improved HIV-1 budding, overall rescue levels were never as high as could be achieved with the attenuated pCMV(Δ4)-CHMP2 expression construct.

We hypothesized that the pCMV(Δ4)-CHMP2A and pCMV(Δ5)-CHMP2A vectors worked well in the rescue experiment because they could be used at concentrations that coupled high transfection efficiencies with restricted protein expression. To test this idea, we created pCMV(WT)-YFP, pCMV(Δ4)-YFP and pCMV(Δ5)-YFP expression vectors and used YFP fluorescence as a measure of protein expression in 293T cells. This approach allowed us to use flow cytometry to quantify transfection efficiencies and relative protein expression levels at the single-cell level. Titrations were again performed to determine the quantity of pCMV(WT)-YFP required to express YFP at levels comparable to those produced by transfections with 500 ng of pCMV(Δ4)-YFP or pCMV(Δ5)-YFP. This was achieved with 19 ng of pCMV(WT)-YFP, in reasonable agreement with the analogous CHMP2A titration experiments (Figure 3A, compare total mean fluorescence levels for 500 ng of pCMV(Δ4)-YFP or pCMV(Δ5)-YFP DNA with 19 ng of pCMV(WT)-YFP). As shown in Figure 3B, overall transfection efficiencies under these three conditions were: 94 ± 1% for 500 ng of pCMV(Δ4)-YFP, 90 ± 2% for 500 ng of pCMV(Δ5)-YFP DNA and 36 ± 8% for 19 ng pCMV(WT)-YFP (compare lanes 2, 3 and 5). Thus, overall transfection efficiencies dropped off significantly when the quantity of vector was reduced from 500 to 19 ng. We also quantified the mean fluorescence intensity (MFI) in the subsets of cells that were actually transfected in each reaction (i.e., now excluding cells in which YFP expression was undetectable). As shown in Figure 3C, transfected cells in the 19 ng pCMV(WT)-YFP reaction had a MFI of

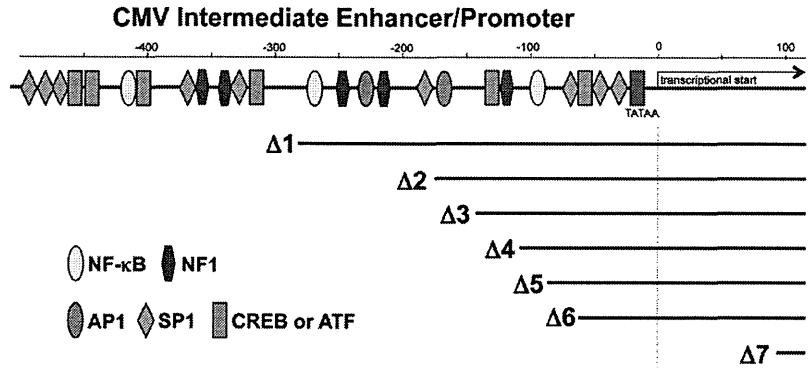

Figure 1. Human cytomegalovirus major immediate early enhancer/promoter constructs used for attenuated gene expression. The human CMV promoter structure is shown above, with the transcription start site at the +1 position and (putative) upstream binding sites for different transcription factors. Promoter deletion positions are shown below. Transcription factor binding elements were identified using the TESS analysis tool (22), with a consensus sequence cutoff of >12.0. Similar but slightly different variants of this binding site map were also generated by the program TFSEARCH (23) and have been published (24). Promoter deletions were introduced by cloning PCR fragments (*MluI*-*XbaI* sites) with the designated deletions into a pcDNA 3.1/myc-His(-)A expression vector (Life Technologies) that carried a custom multicloning site between the *XbaI* and *AflII* sites. Deletion design and DNA sequences are provided in Supplementary Figure 1, and construct numbers are provided in Supplementary Table 1.

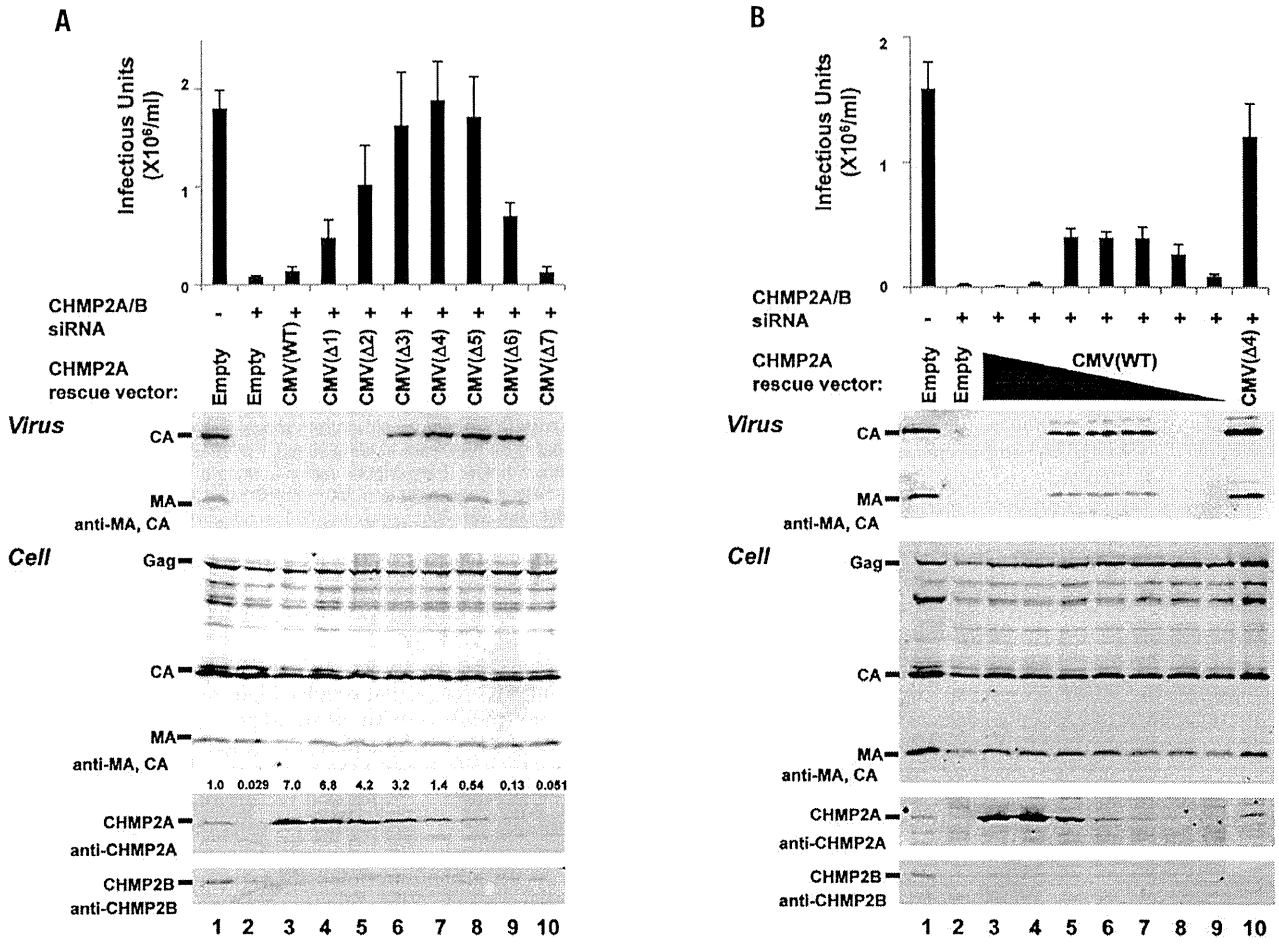

Figure 2. Rescue of HIV-1 budding from 293T cells that lack endogenous CHMP2 proteins by expression of human CHMP2A from attenuated CMV expression vectors. (A) Differential rescue of HIV-1 budding by CHMP2A proteins expressed from the ensemble of different pCMV-CHMP2A expression vectors. HIV-1 vector infectivity titers (top panel) and Western blots showing protein levels in culture supernatants (panel 2) or 293T cells (Cell, panels 3–5) co-transfected with a proviral HIV-1 vector (500 ng of pCMV-dR8.2, 500 ng pLox-GFP, 250 ng pMD-G)(25) (all lanes), either 20 nM control siRNA duplex (CGUACGCGGAAUACUUCGAtt, where "tt" represents two overhanging deoxyribothymidines, lanes 1) or 10 nM each of siRNA duplexes against CHMP2A and CHMP2B (AGGCAGAGAUCAUGGAUAUtt and GGAACAGAAUCGAGAGUUAtt, lanes 2–10)(15), and 500 ng of either an empty vector control (lane 2) or the designated pCMV-CHMP2A vector expressing an siRNA-resistant CHMP2A construct (lanes 3–10). Integrated CHMP2A band intensities, normalized to the endogenous CHMP2A level, are provided over each lane in panel 4. 293T cells (2×10^5 cells/well, 6-well plates, 2 mL volume) were seeded at t = 0, transfected with siRNA (20 nM final total concentration, 7.5 µl Lipofectamine RNAiMAX; Life Technologies, Carlsbad, CA, USA) at t = 24h, and co-transfected with siRNA, the designated pCMV-CHMP2A vector (500 ng), and the HIV-1 vector (20 nM final total siRNA concentration, 500 ng pCMV-dR8.2, 500 ng pLox-GFP, 250 ng pMD-G, 10 µl Lipofectamine 2000; Life Technologies) at t = 48h. The following silent mutations were introduced into the CHMP2A cDNA coding sequence to make the CHMP2A mRNA siRNA resistant: AGGCAGAGATCATGGATAT to AaGCtGAaATtATGGATAT (nucleotides 395–413). Cells and supernatant were collected and analyzed at t = 96h. Released virions were pelleted through a 20% sucrose cushion at 15,000× *g* and viral Gag-derived proteins were detected by Western blotting using our rabbit anti-HIV-1 CA (UT415, 1:2000) and MA (UT556, 1:1000) antisera. Cells were lysed with buffer (50 mM Tris-HCl pH 7.4, 150 mM NaCl, 1% Triton-X100, and PMSF) for Western blotting of intracellular proteins. Anti-CHMP2A and CHMP2B were detected with UT589 (our antibody) and Ab33174 (Abcam, Cambridge, MA, USA) as described (26). Secondary antibodies were anti-mouse IgG or anti-rabbit IgG polyclonal conjugated to IRdye700 or IRdye800 (1:10000, Rockland Immunochemicals Inc., Gilbertsville, PA, USA). Western blots were visualized using an Odyssey scanner (Li-Cor Biosciences, Lincoln, NB, USA). For titer measurements, 293T cells were infected with viral supernatants and GFP-positive cells were quantified by flow cytometry (FL1 channel, FACScan, BD Biosciences, San Jose, CA, USA). Values show the average of three independent repetitions with standard errors. (B) Rescue of HIV-1 budding by CHMP2A proteins expressed from different quantities of the wild type CMV expression vector, pCMV(WT)-CHMP2A. The figure and experiments are equivalent to panel (A), except that the following quantities of the siRNA-resistant CHMP2A rescue construct pCMV(WT)-CHMP2A were transfected: 500 ng (lane 3), 170 ng (lane 4), 56 ng (lane 5), 19 ng (lane 6), 6.2 ng (lane 7), 2.1 ng (lane 8), and 0.69 ng (lane 9). In the experiments shown in lanes 4–9, total expression vector levels were adjusted to 500 ng with pCMV(WT) empty vector. The sample shown in lane 10 was transfected with 500 ng of the pCMV(Δ4)-CHMP2A expression vector (positive control).

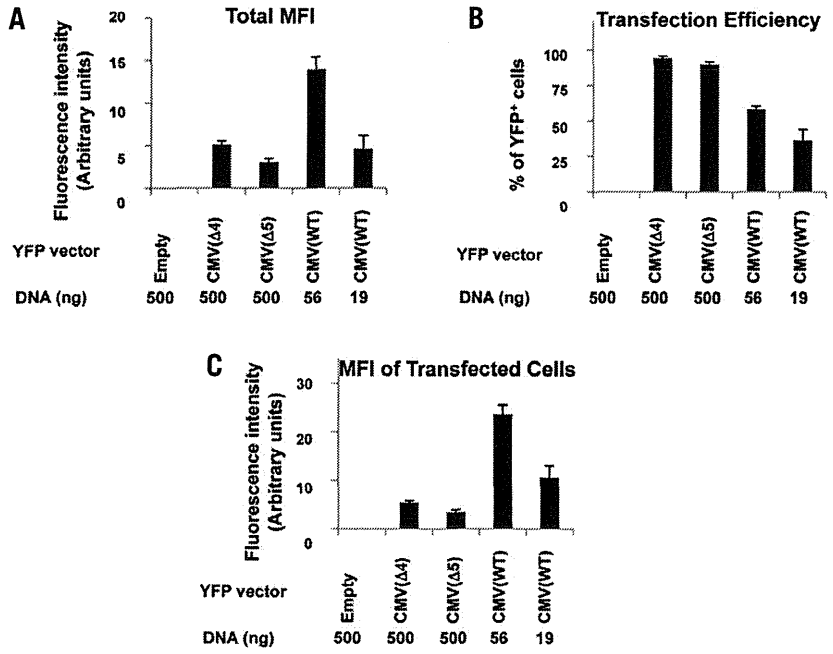

Figure 3. Comparison of transfection efficiencies and protein expression levels for the pCMV(WT)-YFP, pCMV(Δ4)-YFP, and pCMV(Δ5)-YFP vectors. (A) Total mean fluorescence intensity of YFP (MFI, in arbitrary units) for all cells in each of the cultures following transfection with 500 ng empty pCMV(WT) (negative control, lane 1), 500 ng pCMV(Δ4)-YFP (lane 2), 500 ng pCMV(Δ5)-YFP (lane 3), 56 ng pCMV(WT)-YFP (lane 4), or 19 ng pCMV(WT)-YFP (lane 5). The YFP expression vectors were created by PCR amplification of the *yfp* gene and subcloned into the *KpnI*/*XhoI* sites of the custom multiple cloning site of the pcDNA 3.1/myc-His(-)A expression vector. 293T cells were seeded (t = 0, 2×10^5 cells/well, 6-well plates) and transfected (t = 24h) with the designated pCMV-YFP constructs (adjusted to 500 ng total DNA with pCMV(WT) empty vector where necessary), 10 µl Lipofectamine 2000). At t = 72h, cells were trypsinized and analyzed by flow cytometry. YFP-positive cells were scored using a control-transfected sample to set the negative background level (BD CellQuest Pro software). YFP intensity was determined after subtracting control-transfected samples (FL1). Values here and in panels B and C show the average of five independent repetitions with standard errors. (B) Percentages of cells with detectable YFP fluorescence in each of the cultures described in (A). (C) Mean YFP fluorescence intensity (arbitrary units) for the subsets of cells that were transfected (as judged by detectable YFP expression) in each of the cultures described in (A).

11 ± 2, whereas transfected cells in the 500 ng pCMV(Δ4)-YFP and pCMV(Δ5)-YFP reactions had MFI of 5.4 ± 0.4 and 3.4 ± 0.6. These data demonstrate that although bulk YFP expression levels were comparable for the three conditions, this was achieved in different ways: the pCMV(Δ4)-YFP and pCMV(Δ5)-YFP vectors supported low-level YFP expression in nearly all of the cells, whereas the pCMV(WT)-YFP vector supported higher expression levels per cell, but in fewer than half of the cells. Thus, the attenuated vectors appear to work better in rescue experiments because, unlike the wild type pCMV(WT) vector, they can be used at sufficiently high concentrations to maintain high overall transfection efficiencies, yet they express low levels of the target protein in each cell. It is possible that varying HIV-1 vector levels could also affect the degree of rescue, but our experiments did not test this parameter.

In summary, we have created mammalian expression vectors that allow tunable expression of siRNA-resistant constructs and demonstrated their utility in rescuing HIV-1 budding from cells that lacked endogenous CHMP2 proteins. We have also used this system successfully in other experiments, for example to achieve high-level rescue of retrovirus budding from cells depleted of endogenous ALIX and CHMP4 proteins (although the relative advantages of using the attenuated CMV vector system were somewhat less pronounced in these two cases, data not shown). The optimal CMV vector must, of course, be determined empirically for each new system because the correct choice will be influenced by differences in endogenous protein levels, protein expression efficiencies, and the degree to which the specific pathway and cell type can tolerate protein overexpression. Although, we are not aware of previous studies that have employed the approach described here, related approaches such as the use of inducible promoters to optimize the expression of siRNA-resistant rescue constructs have been described (21). In principle, this is an elegant approach that can also be used to maximize phenotypic rescue, but it requires the creation of stable cell lines and is therefore less convenient than transient transfection, particularly when the functions of multiple mutant proteins are being screened. Hence, our system is likely to be most useful in cases where levels of the rescue protein must be tightly controlled and where the creation of stable cell lines is overly time consuming or problematic. Our vectors should also be useful in other applications where it is desirable to attenuate protein expression while maintaining high transfection levels.

Acknowledgments

This work was supported by National Institutes of Health grant AI051174 (W.I.S) and research fellowships from the Japanese Herpesvirus Infections Forum (J.A.) and the Deutsche Forschungsgemeinschaft (J.V., VO 1836/1-1). This paper is subject to the NIH Public Access Policy.

Competing interests

The authors declare no competing interests.

References

1. **Elbashir, S.M., J. Harborth, W. Lendeckel, A. Yalcin, K. Weber, and T. Tuschl.** 2001. Duplexes of 21-nucleotide RNAs mediate RNA interference in cultured mammalian cells. Nature *411*:494-498.
2. **Houzet, L. and K.T. Jeang.** 2011. Genome-wide screening using RNA interference to study host factors in viral replication and pathogenesis. Exp. Biol. Med. (Maywood) *236*:962-967.
3. **Sigoillot, F.D. and R.W. King.** 2011. Vigilance and validation: Keys to success in RNAi screening. ACS Chem. Biol. *6*:47-60.
4. **Falschlehner, C., S. Steinbrink, G. Erdmann, and M. Boutros.** 2010. High-throughput RNAi screening to dissect cellular pathways: a how-to guide. Biotechnol. J. *5*:368-376.
5. **Martin, S.E. and N.J. Caplen.** 2007. Applications of RNA interference in mammalian systems. Annu. Rev. Genomics Hum. Genet. *8*:81-108.
6. **Pache, L., R. Konig, and S.K. Chanda.** 2011. Identifying HIV-1 host cell factors by genome-scale RNAi screening. Methods *53*:3-12.
7. **Sakurai, K., P. Chomchan, and J.J. Rossi.** 2010. Silencing of gene expression in cultured cells using small interfering RNAs. Curr Protoc Cell Biol *Chapter 27*:Unit 27 21 21-28.
8. **Lassus, P., J. Rodriguez, and Y. Lazebnik.** 2002. Confirming specificity of RNAi in mammalian cells. Sci. STKE *2002*:pl13.
9. **Garrus, J.E., U.K. von Schwedler, O.W. Pornillos, S.G. Morham, K.H. Zavitz, H.E. Wang, D.A. Wettstein, K.M. Stray, et al.** 2001. Tsg101 and the vacuolar protein sorting pathway are essential for HIV-1 budding. Cell

107:55-65.
10. **Cullen, B.R.** 2006. Enhancing and confirming the specificity of RNAi experiments. Nat. Methods *3*:677-681.
11. **Henne, W.M., N.J. Buchkovich, and S.D. Emr.** 2011. The ESCRT Pathway. Dev. Cell *21*:77-91.
12. **Martin-Serrano, J. and S.J. Neil.** 2011. Host factors involved in retroviral budding and release. Nat. Rev. Microbiol. *9*:519-531.
13. **Hurley, J.H. and P.I. Hanson.** 2010. Membrane budding and scission by the ESCRT machinery: it's all in the neck. Nat. Rev. Mol. Cell Biol. *11*:556-566.
14. **Dordor, A., E. Poudevigne, H. Gottlinger, and W. Weissenhorn.** 2011. Essential and supporting host cell factors for HIV-1 budding. Future Microbiol. *6*:1159-1170.
15. **Morita, E., V. Sandrin, J. McCullough, A. Katsuyama, I. Baci Hamilton, and W.I. Sundquist.** 2011. ESCRT-III Protein Requirements for HIV-1 Budding. Cell Host Microbe *9*:235-242.
16. **Howard, T.L., D.R. Stauffer, C.R. Degnin, and S.M. Hollenberg.** 2001. CHMP1 functions as a member of a newly defined family of vesicle trafficking proteins. J. Cell Sci. *114*:2395-2404.
17. **von Schwedler, U.K., M. Stuchell, B. Muller, D.M. Ward, H.Y. Chung, E. Morita, H.E. Wang, T. Davis, et al.** 2003. The protein network of HIV-1 budding. Cell *114*:701-713.
18. **Martin-Serrano, J., A. Yaravoy, D. Perez-Caballero, and P.D. Bieniasz.** 2003. Divergent retroviral late-budding domains recruit vacuolar protein sorting factors by using alternative adaptor proteins. Proc. Natl. Acad. Sci. USA *100*:12414-12419.
19. **Strack, B., A. Calistri, S. Craig, E. Popova, and H.G. Gottlinger.** 2003. AIP1/ALIX Is a Binding Partner for HIV-1 p6 and EIAV p9 Functioning in Virus Budding. Cell *114*:689-699.
20. **Zamborlini, A., Y. Usami, S.R. Radoshitzky, E. Popova, G. Palu, and H. Gottlinger.** 2006. Release of autoinhibition converts ESCRT-III components into potent inhibitors of HIV-1 budding. Proc. Natl. Acad. Sci. USA *103*:19140-19145.
21. **Ma, H.T. and R.Y. Poon.** 2010. Gene down-regulation with short hairpin RNAs and validation of specificity by inducible rescue in mammalian cells. Curr Protoc Cell Biol *Chapter 27*:Unit 27 22.
22. **Schug, J.** 2009. Using TESS to predict transcription factor binding sites in DNA sequence*In* A.D. Baxevanis (Ed.), Current Protocols in Bioinformatics. John Wiley & Sons, Ltd.
23. **Heinemeyer, T., E. Wingender, I. Reuter, H. Hermjakob, A.E. Kel, O.V. Kel, E.V. Ignatieva, E.A. Ananko, et al.** 1998. Databases on transcriptional regulation: TRANSFAC, TRRD and COMPEL. Nucleic Acids Res. *26*:362-367.
24. **Stinski, M.F. and H. Isomura.** 2008. Role of the cytomegalovirus major immediate early enhancer in acute infection and reactivation from latency. Med. Microbiol. Immunol. (Berl.) *197*:223-231.
25. **Naldini, L., U. Blomer, F.H. Gage, D. Trono, and I.M. Verma.** 1996. Efficient transfer, integration, and sustained long-term expression of the transgene in adult rat brains injected with a lentiviral vector. Proc. Natl. Acad. Sci. USA *93*:11382-11388.
26. **Morita, E., L.A. Colf, M.A. Karren, V. Sandrin, C.K. Rodesch, and W.I. Sundquist.** 2010. Human ESCRT-III and VPS4 proteins are required for centrosome and spindle maintenance. Proc. Natl. Acad. Sci. USA *107*:12889-12894.

Received 15 June 2012; accepted 13 July 2012.

Address correspondence to: Wesley I. Sundquist, Department of Biochemistry, 15 N. Medical Drive, Room 4100, University of Utah School of Medicine, Salt Lake City, UT, USA. Email: wes@biochem.utah.edu

Journal of proteome research

Article

pubs.acs.org/jpr

Proteomic Analysis of Hepatitis C Virus (HCV) Core Protein Transfection and Host Regulator PA28γ Knockout in HCV Pathogenesis: A Network-Based Study

Lokesh P. Tripathi,[†,∥] Hiroto Kambara,[‡,∥] Kohji Moriishi,[‡] Eiji Morita,[‡] Takayuki Abe,[‡] Yoshio Mori,[‡] Yi-An Chen,[†,§] Yoshiharu Matsuura,[‡] and Kenji Mizuguchi*[,†,§]

[†]National Institute of Biomedical Innovation, 7-6-8 Saito Asagi, Ibaraki, Osaka, 567-0085, Japan

[‡]Department of Molecular Virology, Research Institute for Microbial Diseases and [§]Graduate School of Frontier Biosciences, Osaka University, 3-1 Yamada-Oka, Suita, Osaka, 565-0871, Japan

S *Supporting Information*

ABSTRACT: Hepatitis C virus (HCV) causes chronic liver disease worldwide. HCV Core protein (Core) forms the viral capsid and is crucial for HCV pathogenesis and HCV-induced hepatocellular carcinoma, through its interaction with the host factor proteasome activator PA28γ. Here, using BD-PowerBlot high-throughput Western array, we attempt to further investigate HCV pathogenesis by comparing the protein levels in liver samples from Core-transgenic mice with or without the knockout of PA28γ expression (abbreviated PA28γ$^{-/-}$CoreTG and CoreTG, respectively) against the wild-type (WT). The differentially expressed proteins integrated into the human interactome were shown to participate in compact and well-connected cellular networks. Functional analysis of the interaction networks using a newly developed data warehouse system highlighted cellular pathways associated with vesicular transport, immune system, cellular adhesion, and cell growth and death among others that were prominently influenced by Core and PA28γ in HCV infection. Follow-up assays with *in vitro* HCV cell culture systems validated VTI1A, a vesicular transport associated factor, which was upregulated in CoreTG but not in PA28γ$^{-/-}$CoreTG, as a novel regulator of HCV release but not replication. Our analysis provided novel insights into the Core-PA28γ interplay in HCV pathogenesis and identified potential targets for better anti-HCV therapy and potentially novel biomarkers of HCV infection.

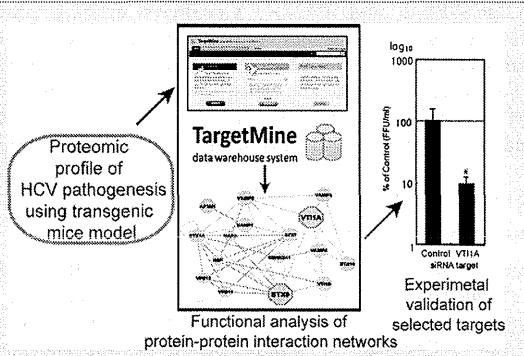

KEYWORDS: *CoreTG, GO, HCC, HCV, KEGG, OMIM, PA28γ$^{-/-}$CoreTG, PPI, siRNA, TargetMine*

INTRODUCTION

Hepatitis C virus (HCV) is a prime cause of chronic liver disease frequently characterized by liver inflammation with accompanying steatosis, progressive fibrosis, and hepatocellular carcinoma (HCC) and infects nearly 3% of the world's population. HCV contains a single-stranded RNA genome encoding a 3000-amino-acid polyprotein, which is processed by host and viral factors to yield 10 viral proteins, Core, E1, E2, p7, NS2, NS3, NS4A, NS4B, NS5A, and NS5B.[1−4] HCV variants are classified into six major genotypes with multiple subtypes characterized by phylogenetic heterogeneity, differences in infectivity, and interferon sensitivity.[5,6] The availability of cell-culture-based systems for HCV infection has provided an increased understanding of HCV pathogenesis.[5,7−9] Transgenic mice (preferably C57BL strain) expressing HCV proteins in the liver are also a preferred choice for the investigation of HCV pathogenesis.[10] However, despite considerable research efforts, precise molecular mechanisms underlying HCV pathology remain unclear.

HCV Core protein (hereafter referred to as Core) is spliced from the polyprotein by the signal peptidase and further processed into a highly conserved 21-kDa mature form by the signal peptide peptidase; this processing facilitates its transfer to the detergent-resistant membrane fraction where virus replication and assembly take place. Core is a multifunctional protein implicated in RNA binding and as a pathogenic factor; it induces steatosis and HCC and, thus, liver failure.[1,10] The ubiquitin-proteasome pathway, the premier intracellular protein degradation system in eukaryotes, is a key regulator of cellular processes and is also associated with the evasion of host immune response by many viruses, viral maturation, and progeny release.[11] Core binds to the proteasome activator PA28γ in the nucleus and is degraded via a PA28γ-dependent pathway. PA28γ plays a crucial role in Core-induced insulin resistance, steatogenesis, and hepatocarcinogenesis and in HCV propagation; PA28γ knockout in Core transgenic mice disrupts

Received: February 7, 2012
Published: May 31, 2012

steatosis and HCC, restores insulin sensitivity, and impairs viral particle production, and thus PA28γ is a promising target for anti-HCV therapies with minimal side effects.[2,12−15] However, the exact mechanisms through which PA28γ facilitates Core-induced HCV pathogenesis remain poorly understood.

In this study, we aim to put forth biological networks that describe the differential expression of the host proteins and their likely roles in modulating PA28γ function in HCV pathogenesis. We employed PowerBlot Western Array screening system, a high-throughput Western blotting method, to identify changes at the proteome level in Core expressing transgenic C57BL/6 mice with or without the knockout of PA28γ gene expression (abbreviated PA28γ$^{-/-}$CoreTG and CoreTG, respectively). In our analysis, we included human protein interaction data and gene regulatory information for the differentially expressed proteins using TargetMine, an integrated data warehouse that we have developed recently.[16] Our network-based analyses of the proteomic changes from the three data sets (CoreTGvsC57BL/6, PA28γ$^{-/-}$CoreTGvsC57BL/6 and PA28γ$^{-/-}$CoreTGvsCoreTG) provided novel insights into PA28γ function in Core-induced HCV pathogenesis. Furthermore, we identified VTI1A, a vesicular transport associated factor, which was upregulated in CoreTG but not in PA28γ$^{-/-}$CoreTG, as a novel regulator of HCV release and, thus, an attractive target for anti-HCV therapy.

MATERIALS AND METHODS

Protein Sample Preparation

Protein samples were prepared from the livers of the C57BL/6 wild-type (hereafter referred to as WT) and the transgenic mice expressing HCV Core protein genotype 1b line C49 with (PA28γ$^{-/-}$CoreTG) or without (CoreTG) the knockout of PA28γ expression.[2,12] Livers were harvested from three individuals each of WT, CoreTG, and PA28γ$^{-/-}$CoreTG mice, and the harvested samples for each mice type were pooled together prior to protein sample preparation for PowerBlot analysis. The pooled liver samples of each mice type were homogenized in 1x sample buffer of SDS-PAGE on ice and then boiled for 5 min. The boiled sample was sonicated for the viscosity of DNA and employed for PowerBlot analysis.

PowerBlot Western Array Analysis

The levels of differentially expressed proteins were determined by the PowerBlot assay by BD Biosciences Pharmingen (San Diego, CA, USA). Briefly, samples containing 200 μg of protein was loaded in one big well on top of a 4−15% gradient SDS-polyacrylamide gel and separated by electrophoresis (1.5 h at 150v). The proteins were transferred to Immobilon-FL membrane (Millipore, Billerica, MA, USA) for 2 h at 200 mA. After transfer, the membranes were incubated in the blocking buffer (LI-COR, Lincoln, NE, USA). The membrane was clamped with a Western blotting manifold that isolates 41 channels across the membrane. Each channel was incubated with a complex antibody cocktail for 1 h. The blots were removed from the manifold, washed, and hybridized for 30 min with secondary goat anti-mouse antibody conjugated to Alexa680 fluorescent dye (Molecular Probes, Eugene, OR, USA). Image data were captured using the Odyssey Infrared Imaging System (LI-COR). Data analysis included the raw and normalized signal intensity data from each blot. The results were expressed as fold change that represented the protein changes, either increasing or decreasing in the comparative analysis between the experimental samples and the control. The detected protein expression changes were listed in the order of confidence, 0 through 3, with 3 being the highest level of confidence, based on the signal quality. Only the data from confidence levels 2 and 3 (good quality signals; Supporting Information; Tables S1, S2a, S2b, and S2c) for proteins mapped to valid accessions were considered for further analysis. Proteins that displayed >1.8-fold change in abundance were judged to be differentially expressed, following the manufacturer's recommendation.

Human Orthologues for the Differentially Expressed Proteins

BD PowerBlot assay employs a cocktail of monoclonal antibodies that target human, mouse, and rat proteins, and in a specific study, over 90% were found to cross-react with proteins from human, mouse and rat[17] (Table S1). Human orthologues for the proteins picked up by the antibody cocktail were retrieved from KEGG (Tables S2a, S2b, and S2c).

Construction of Protein−Protein Interaction Networks

PPIs for the human orthologues of each set of differentially expressed proteins were retrieved from BioGRID 3.1.74[18] and iRefIndex 8.0[19] databases along with the interactions between the primary interactors of the differentially expressed proteins using TargetMine.[16] TargetMine is an integrated data warehouse that combines different biological data types and employs an objective protocol to prioritize candidate genes for further experimental investigation.[16] The interactions were merged and filtered for redundancy to infer overall extended PPI networks. Protein identifiers used in the different databases were mapped to Entrez gene IDs and official gene symbols. The official gene symbols are used hereafter, to refer to the differentially expressed proteins (Table 1) and their interacting partners. All the relationships discussed should be interpreted as protein relationships unless otherwise clarified.

PPI Network Topological Analysis

Network components were visualized using Cytoscape 2.6,[20] while network properties such as *node degree distribution* and *shortest path* measures were computed using the Cytoscape NetworkAnalyzer plugin[21] as described previously.[22] In a PPI network, the degree of a node (protein) is defined as the number of nodes directly connected to (interacting with) it, i.e., its first neighbors. *Node degree distribution*, $P(k)$, is the number of nodes with a degree k for $k = 0, 1, 2, \ldots$. The *shortest path length* between two nodes n and m, $L(n,m)$, is the minimal number of interactions that link proteins n and m in a PPI network. The *shortest path length distribution* is the number of node pairs (n,m) with $L(n,m) = x$ for $x = 1, 2, \ldots$. The *average shortest path length*, also known as the *characteristic path length*, gives the expected distance between two connected nodes i.e. the minimal number of interactions that link any two proteins in a PPI network.

Functional Analysis by Characterization of Enriched Biological Associations

Gene ontology (GO) associations retrieved from GO consortium,[23] biological pathway data from KEGG (retrieved on March 1, 2011),[24] and disease phenotype associations from OMIM[25] were used to assign functional annotations to the constituents of the extended PPI networks. The proteins in each of the extended PPI networks were uploaded to TargetMine to create protein lists, and the enrichment of specific biological themes (GO terms, KEGG Pathways, OMIM phenotypes) associated with each PPI network was estimated

dx.doi.org/10.1021/pr300121a | J. Proteome Res. 2012, 11, 3664−3679

Table 1. Summary of PowerBlot Detected Protein Expression Levels in Protein Samples

CoreTGvsWT					
protein	gene ID	symbol	confidence level[a]	(−) under, (+) over[b]	fold change[c]
P31749	207	AKT1	3	−	2.68
P07355	302	ANXA2	3	+	2.92
O43747	164	AP1G1	3	+	5.72
P63010	163	AP2B1	3	+	2.40
Q96CW1	1173	AP2M1	2	+	1.93
Q9Y2T2	26985	AP3M1	2	+	1.89
P05089	383	ARG1	2	+	2.08
P52566	397	ARHGDIB	3	+	2.02
O15145	10094	ARPC3	2	−	2.25
P49407	408	ARRB1	3	−	2.33
Q07812	581	BAX	3	+	2.03
P55212	839	CASP6	3	−	1.95
Q14790	841	CASP8	2	+	2.18
Q03135	857	CAV1	2	+	2.07
P12830	999	CDH1	3	−	2.33
P19022	1000	CDH2	3	+	4.57
Q53SH4	1134	CHRNA1	3	−	3.11
P21964	1312	COMT	2	+	2.96
P00450	1356	CP	3	+	2.36
P21291	1465	CSRP1	3	+	2.23
P49711	10664	CTCF	3	+	6.13
P25685	3337	DNAJB1	3	−	2.16
P63241	1984	EIF5A	3	+	1.94
P42566	2060	EPS15	3	+	4.28
Q92889	2072	ERCC4	3	+	5.43
O75899	9568	GABBR2	3	+	3.39
O43719	27336	HTATSF1	3	+	5.76
P06756	3685	ITGAV	3	+	6.32
Q14974	3837	KPNB1	3	−	1.86
Q16539	1432	MAPK14	3	−	2.81
Q9UPY8	22924	MAPRE3	3	+	2.46
P49736	4171	MCM2	3	+	1.87
P62166	23413	NCS1	3	−	2.24
Q8IZS7	140767	NRSN1	3	+	1.89
Q16620	4915	NTRK2	3	+	2.40
Q14980	4926	NUMA1	3	−	1.94
P07237	5034	P4HB	3	+	2.27
Q92878	10111	RAD50	3	+	4.93
Q99638	5883	RAD9A	2	−	3.10
P20936	5921	RASA1	3	+	1.86
Q96SB4	6732	SRPK1	3	+	3.11
Q92186	8128	ST8SIA2	3	+	5.11
P42224	6772	STAT1	3	+	2.00
P40763	6774	STAT3	3	+	2.30
Q9UNK0	9482	STX8	3	+	1.88
Q12800	7024	TFCP2	3	+	5.04
Q92752	7143	TNR	3	+	5.36
Q13263	10155	TRIM28	3	+	4.70
O43396	9352	TXNL1	3	−	4.82
P50552	7408	VASP	2	−	2.61
Q96AJ9	143187	VTI1A	3	+	3.25
Q14191	7486	WRN	3	+	17.12

altered protein levels in PA28γ$^{-/-}$CoreTGvsWT					
protein	gene ID	symbol	confidence level[a]	(−) under, (+) over[b]	fold change[c]
O15145	10094	ARPC3	2	−	1.96
P49407	408	ARRB1	3	−	2.17
P55212	839	CASP6	3	−	2.04

altered protein levels in PA28γ$^{-/-}$CoreTGvsWT					
protein	gene ID	symbol	confidence level[a]	(−) under, (+) over[b]	fold change[c]
O60508	51362	CDC40	2	+	1.99
P54105	1207	CLNS1A	3	+	2.41
P21964	1312	COMT	2	+	2.71
P67870	1460	CSNK2B	3	+	1.90
P78352	1742	DLG4	2	+	4.08
Q95GK7	1837	DTNA	3	−	2.42
P55010	1983	EIF5	3	+	2.19
Q08495	2039	EPB49	3	+	2.66
P37268	2222	FDFT1	2	+	5.68
P09038	2247	FGF2	2	+	2.69
P62962	2280	FKBP1A	2	+	1.89
O75146	9026	HIP1R	2	−	2.08
Q9NZL4	23640	HSPBP1	3	+	3.46
P05412	3725	JUN	2	+	2.15
P52292	3838	KPNA2	3	−	7.28
P36507	5605	MAP2K2	3	−	2.35
Q16539	1432	MAPK14	3	−	3.29
P22033	4594	MUT	3	+	2.46
P54920	8775	NAPA	2	−	1.97
Q8IZS7	140767	NRSN1	3	+	1.93
Q16620	4915	NTRK2	3	+	2.50
P07237	5034	P4HB	3	+	2.04
Q08209	5530	PPP3CA	3	+	7.55
Q06124	5781	PTPN11	2	+	2.33
Q99638	5883	RAD9A	2	−	1.97
P43487	5902	RANBP1	3	+	2.29
Q9UPX8	22941	SHANK2	3	−	1.94
P29353	6464	SHC1	3	+	3.27
Q92186	8128	ST8SIA2	3	+	4.06
P31948	10963	STIP1	3	−	1.99
O75558	8676	STX11	2	+	2.04
P23193	6917	TCEA1	3	−	2.17
P07101	7054	TH	2	+	2.78
P13693	7178	TPT1	3	−	1.93
Q15628	8717	TRADD	3	−	2.00
P50607	7275	TUB	3	+	1.91

altered protein levels in PA28γ$^{-/-}$CoreTGvsCoreTG					
protein	gene ID	symbol	confidence level[a]	(−) under, (+) over[b]	fold change[c]
P07355	302	ANXA2	3	−	2.96
O43747	164	AP1G1	3	−	4.20
P63010	163	AP2B1	3	−	3.01
Q96CW1	1173	AP2M1	2	−	1.88
Q9Y2T2	26985	AP3M1	3	+	2.38
O00499	274	BIN1	2	−	1.88
Q9UQM7	815	CAM2KA	3	+	2.06
Q8N5S9	84254	CAMKK1	2	+	5.78
P19022	1000	CDH2	3	−	3.85
P25108	1134	CHRNA1	3	+	2.55
P49674	1454	CSNK1E	3	+	1.97
P67870	1460	CSNK2B	3	+	1.88
P21291	1465	CSRP1	3	+	1.87
P49711	10664	CTCF	3	−	5.43
Q8WTW3	9382	COG1	3	−	7.02
P00450	1356	CP	3	−	3.55
Q13618	8452	CUL3	3	+	1.91
P78352	1742	DLG4	2	+	2.13
Q9Y4J8	1837	DTNA	3	−	2.94

dx.doi.org/10.1021/pr300121a | J. Proteome Res. 2012, 11, 3664−3679

Table 1. continued

altered protein levels in PA28γ⁻/⁻CoreTGvsCoreTG					
protein	gene ID	symbol	confidence level[a]	(−) under, (+) over[b]	fold change[c]
Q08495	2039	EBP49	3	+	2.30
O14682	8507	ENC1	3	+	2.88
P42566	2060	EPS15	3	−	2.11
Q92889	2072	ERCC4	3	−	3.49
P09038	2247	FGF2	2	−	2.18
P62962	2280	FKBP1A	2	+	2.59
P49356	2342	FNTB	2	+	1.95
O75899	9568	GABBR2	3	−	2.53
O75146	9026	HIP1R	3	−	1.97
Q9NZL4	23640	HSPBP1	3	+	3.60
P61604	3336	HSPE1	3	−	2.17
Q99730	27336	HTATSF1	3	−	9.24
Q9Y6K9	8517	IKBKG	2	+	1.97
P52292	3838	KPNA2	3	−	3.94
P36507	5605	MAP2K2	3	−	2.66
Q13505	4580	MTX1	3	−	1.90
P62166	23413	NCS1	3	+	2.56
Q14980	4926	NUMA1	2	+	1.87
P41236	5504	PPP1R2	3	−	2.25
Q08209	5530	PPP3CA	3	+	12.94
P13861	5576	PRKAR2A	3	−	1.88
Q15276	9135	RABEP1	2	−	2.74

altered protein levels in PA28γ⁻/⁻CoreTGvsCoreTG					
protein	gene ID	symbol	confidence level[a]	(−) under, (+) over[b]	fold change[c]
Q92878	10111	RAD50	3	−	5.19
P20936	5921	RASA1	3	+	2.50
P06400	5925	RB1	3	+	2.50
Q92854	10507	SEMA4D	2	+	2.00
Q92529	53358	SHC3	3	−	1.90
P63208	6500	SKP1	3	−	2.45
P43004	6506	SLC1A2	2	+	2.27
Q4U2R8	9356	SLC22A6	3	−	2.23
P42224	6772	STAT1	3	−	1.90
P31948	10963	STIP1	3	−	1.98
O75558	8676	STX11	2	+	3.52
Q8IZU3	50511	SYCP3	3	+	1.88
P07101	7054	TH	2	+	2.62
Q92752	7143	TNR	3	−	4.62
O43396	9352	TXNL1	2	+	3.05
P13693	7178	TPT1	3	−	2.85
Q13263	10155	TRIM28	3	−	3.53
Q15628	8717	TRADD	3	−	2.98
P50607	7275	TUB	3	+	1.96
P41542	8615	USO1	3	−	2.05
Q14191	7486	WRN	3	−	3.44

[a]Defined as follows: Level 3 = changes greater than 2-fold from good quality signals that also pass a visual inspection. Level 2 = changes greater than 2-fold from good quality signals that do not pass a visual inspection. [b]+ indicates an increase in protein level in the experimental sample relative to control. − indicates a decrease in protein level in the experimental sample relative to control. [c]A semiquantitative value that represents the general trend of protein changes for the experimental sample relative to control.

by performing the hypergeometric test within TargetMine.[16] The inferred *p*-values were further adjusted for multiple test correction to control the false discovery rate using the Benjamini and Hochberg procedure,[26,27] and the annotations/pathways were considered significant if $p \leq 0.05$.

Transcription Factor-Target Associations

Transcription factor (TF)-target associations for the differentially expressed proteins were retrieved from the TF-target repository compiled from Amadeus[28] and ORegAnno[29] in TargetMine[16] and are discussed in the Supporting Information.

RNAi and Transfection

The siRNA pair targets to VTI1A, STX8, and COMT were purchased from Ambion (Ambion, Austin, TX, USA). Stealth RNAi Negative Control Low GC Duplex (Invitrogen, Carlsbad, CA, USA) was used as a control siRNA. Each siRNA duplex was introduced into the cell lines by using lipofectamine RNAiMax (Invitrogen). Ambion ID numbers of siRNA duplex of VTI1A and STX8 were S225671 and S18183, respectively. The replicon cell line, as will be described below, was transfected with each siRNA at a final concentration of 20 nM as per the manufacturer's protocol and then seeded at 2.5×10^4 cells per well of a 24-well plate. The transfected cells were harvested at 72 h post-transfection. The Huh7OK1 cell line, as will be described below, was transfected with each siRNA at a final concentration of 20 nM as per the manufacturer's protocol and then seeded at 2.5×10^4 cells per well of a 24-well plate. The transfected cells were infected with JFH1 at an MOI of 0.05 at 24 h post-transfection. The resulting cells were harvested at the indicated time.

Quantitative Reverse-Transcription PCR (qRT-PCR)

Total RNA was prepared from the cell and culture supernatant using the RNeasy mini kit (QIAGEN, Hilden, Germany) and QIAamp Viral RNA Mini Kit (QIAGEN), respectively. First-strand cDNA was synthesized using a high capacity cDNA reverse transcription kit (Applied Biosystems, Carlsbad, CA, USA) with random primers. Each cDNA was estimated by Platinum SYBR Green qPCR Super Mix UDG (Invitrogen) as per the manufacturer's protocol. Fluorescent signals of SYBR Green were analyzed with ABI PRISM 7000 (Applied Biosystems). The HCV internal ribosomal entry site (IRES) region and human glyceraldehyde-3-phosphate dehydrogenase (GAPDH) gene were amplified with the primer pairs 5′-GAGTGTCGTGCAGCCTCCA-3′ and 5′-CACTCGCAAGCACCCTATCA-3′, and 5′-GAAGGTCGGAGTCAACGGATT-3′ and 5′-TGATGACAAGCTTCCCGTTCTC-3′, respectively.[30] The quantities of the HCV genome and the other host mRNAs were normalized with that of GAPDH mRNA. VTI1A and STX8 genes were amplified using the primer pairs 5′-TGACAGGGATGTTGCGAAGA-3′ and 5′-CAACCCACATGCAAACAGGA-3′, and 5′-TTGAAGGGGACCGAAGACAGAACCTC-3′, and 5′-TCAAAACCCAAGCCTCTGGTCTCCT-3′, respectively.

Cell Lines and Virus Infection

Cells from the Huh7OK1 cell line are highly permissive to HCV JFH1 strain (genotype 2a) infection compared to Huh 7.5.1 and exhibit the highest propagation efficiency for JFH1.[30] These cells were maintained at 37 °C in a humidified atmosphere and 5% CO_2, in Dulbecco's modified Eagle's medium (DMEM) (Sigma, St. Louis, MO, USA) supplemented with nonessential amino acids (NEAA), sodium pyruvate, and

dx.doi.org/10.1021/pr300121a | J. Proteome Res. 2012, 11, 3664−3679